Slip-weakening behavior during the propagation of dynamic ruptures obeying rate- and state-dependent friction laws

Andrea Bizzarri and Massimo Cocco

Istituto Nazionale di Geofisica e Vulcanologia, Sezione di Sismologia e Tettonofisica, Rome, Italy

[1]   We model the traction evolution and shear stress degradation near the tip of a propagating dynamic rupture by solving the elastodynamic equation for a 2-D in-plane fault obeying rate- and state-dependent friction laws and adopting a finite difference numerical method. Modeling results clearly show that our dynamic solution implies a slip dependence of fault friction, as previously observed either in laboratory experiments or in theoretical models. However, the resulting equivalent slip-weakening distance (d_0^{eq}) is different from the length scale parameter (L) characteristic of the rate and state formulation. We demonstrate that the state variable evolution controls the slip acceleration and the absorbed fracture energy. The adopted constitutive parameters a, b, and L affect the traction dependence on slip. We present the results of several numerical simulations, performed after a careful control of the available resolution of the cohesive zone, to unravel the dependence of the equivalent slip-weakening distance on the constitutive parameters. We also propose analytical relations to interpret our numerical results, which point out that the traction evolution within the cohesive zone cannot be prescribed a priori in the framework of rate-and-state constitutive laws. In particular, the yield stress and the kinetic friction level depend on particular slip velocity values characteristic of specific stages of the breakdown process. Finally, we discuss how the adopted evolution law affects the slip-weakening curve by comparing the simulations performed with a slip and a slowness law. The former yields smaller equivalent slip-weakening distances than the latter.   *INDEX TERMS:* 7209 Seismology: Earthquake dynamics and mechanics; 7212 Seismology: Earthquake ground motions and engineering; 7215 Seismology: Earthquake parameters; 7260 Seismology: Theory and modeling; *KEYWORDS:* friction laws, earthquake dynamic ruptures, slip-weakening, cohesive zone

1.   Introduction

[2]   Constitutive laws govern fault friction during the nucleation and propagation of earthquake ruptures and are required to have a finite fracture energy absorbed at the crack tip. The relation between the adopted friction law and the total dynamic traction represents one of the fundamental equations to be solved to model spontaneous dynamic ruptures. In the literature two main classes of constitutive formulations have been proposed: the slip-dependent and the rate- and state-dependent (RS) friction laws. The former assumes that friction only depends on slip, while the latter considers that friction depends on slip velocity and state variables. The first class of constitutive models includes the "classical" slip weakening (SW) law [*Barenblatt*, 1959; *Ida*, 1972; *Palmer and Rice*, 1973; *Andrews*, 1976a, 1976b], although other modified slip-weakening behaviors have been proposed including a slip-hardening phase and an exponential decrease of traction with displacement [see *Ohnaka*, 1996, and

references therein]. The second class of constitutive equations is based on the laboratory derived friction laws, which were originally proposed by *Dieterich* [1979, 1986] [see also *Ruina*, 1980, 1983; *Perrin et al.*, 1995]. These two constitutive formulations can both be applied to model the dynamic crack propagation [see *Bizzarri et al.*, 2001, and references therein], but they provide a completely different description of the nucleation process [see *Dieterich*, 1992; *Ohnaka and Shen*, 1999] and the healing mechanisms [*Beeler and Tullis*, 1996; *Bizzarri et al.*, 2001]. The main difference between these two constitutive formulations concerns the time dependence of friction: in fact only rate- and state-dependent friction laws consider an evolution equation for the state variable that yields a more complex time dependency of friction and accounts for fault restrengthening. Therefore RS laws are suitable to model the faulting process and repeated slip episodes on the fault.

[3]   Slip weakening is a characteristic feature of rate- and state-dependent constitutive laws [*Okubo and Dieterich*, 1984; *Guatteri and Spudich*, 2000; *Cocco and Bizzarri*, 2002] because it describes the dynamic traction drop associated with slip acceleration, which is a consequence

of a dynamic failure process occurring at the crack tip in a finite extended zone, named the cohesive zone [*Ida*, 1972; *Andrews*, 1976a, 1976b; *Ohnaka*, 1996]. Therefore these two constitutive laws should not be considered as alternative, at least to describe the dynamic propagation during a single rupture event. However, an important question arising from these considerations is what controls the slip weakening behavior within the cohesive zone; or which are the physical processes controlling the evolution of the dynamic traction, and the consequent slip acceleration, during the breakdown process? Adopting a SW law implicitly means that the traction evolution in the cohesive zone is assigned a priori and it represents the most important phenomenon to be considered to model earthquake propagation and the genesis of seismic waves [see, e.g., *Fukuyama and Madariaga*, 1998]. On the contrary, in the framework of RS constitutive laws slip weakening might be considered as the result of a physical process associated with the frictional control of dynamic rupture growth. In this paper we aim to contribute to this debate.

[4] According to these considerations it is clear that, in order to simulate the dynamic rupture propagation during a single earthquake [see, e.g., *Olsen et al.*, 1997; *Fukuyama and Madariaga*, 1998] with spontaneous models, the adoption of a SW law has the important advantage to prescribe the dynamic traction evolution within the cohesive zone. This is exactly what is needed to allow the crack to advance, the rupture to propagate and to generate seismic waves. However, this does not answer to the questions proposed before on the origin of weakening processes. In this study we attempt to answer to these questions and to study the dynamic rupture propagation and the breakdown processes occurring within the cohesive zone by using a 2-D in plane spontaneous crack model obeying the RS law with a slowness evolution equation.

2. Methodology

[5] In this work we solve the elastodynamic fundamental equation

$$\rho \ddot{u}_i = \sigma_{ij,j} + f_i \qquad (1)$$

for a 2-D in-plane shear crack for which the displacement and the shear traction depend on time and on only one spatial coordinate; we also neglect the body forces ($f_i = 0$). In equation (1), ρ is the mass density, u is the displacement, and $\sigma_{ij,j}$ is the spatial derivative of the stress tensor components. In particular, we assume that the crack propagates only in the x_1 direction and the fault lies on the $x_3 = 0$ plane. A grid of nodes is introduced, and each node is a vertex of an equilateral triangle; the slip velocity components are staggered both in space and time with respect to the total shear stress components σ_{ij}. The latter are defined in the center of the triangles and at integer time steps, while the former are defined in the vertexes of the triangles and at intermediate time steps. The medium is supposed to be infinite, homogeneous and elastic everywhere except along the fracture line. We solve equation (1) by using a finite difference (FD) approach with the traction

at split nodes (TSN) fault boundary condition, described by *Andrews* [1973, 1999]:

$$\rho \frac{\partial}{\partial t} \dot{u}_1 = \frac{\partial}{\partial x_1} \sigma_{11} + \frac{\partial}{\partial x_2} \sigma_{12}$$
$$\rho \frac{\partial}{\partial t} \dot{u}_2 = \frac{\partial}{\partial x_1} \sigma_{12} + \frac{\partial}{\partial x_2} \sigma_{22}. \qquad (2)$$

The details of the numerical solution are described by *Bizzarri et al.* [2001]. We can use in our procedure either RS laws with slowness (ageing) evolution equation [*Dieterich*, 1986]:

$$\tau = \left[\mu_* - a \ln\left(\frac{v_*}{v} + 1\right) + b \ln\left(\frac{\Phi v_*}{L} + 1\right) \right] \sigma_n^{\text{eff}} \qquad (3a)$$

$$\frac{d}{dt}\Phi = 1 - \frac{\Phi v}{L} \qquad (3b)$$

or with slip evolution equation [*Beeler et al.*, 1994; *Roy and Marone*, 1996]:

$$\tau = \left[\mu_* + a \ln\left(\frac{v}{v_*}\right) + b \ln\left(\frac{\Theta v_*}{L}\right) \right] \sigma_n^{\text{eff}} \qquad (4a)$$

$$\frac{d\Theta}{dt} = -\frac{\Theta v}{L} \ln\left(\frac{\Theta v}{L}\right). \qquad (4b)$$

In equations (3) and (4), v is the slip velocity, μ_* and v_* are arbitrary reference values for the friction coefficient and for the slip velocity, respectively; a, b, and L are the three constitutive parameters, and s_n^{eff} is the effective normal stress. The quantities Φ and Θ are the state variables. These two rate- and state-dependent laws differ only for the evolution relation, which defines the temporal behavior of the state variable. In this formulation, the state variable has the physical meaning of an average contact time between the sliding surfaces [*Dieterich*, 1986; *Ruina*, 1983]. The evolution equation (3b) is the slowness law [*Beeler et al.*, 1994; *Roy and Marone*, 1996], and it includes true ageing, while that included in equation (4b) is named the slip law. In this work we consider a velocity-weakening behavior (that is, $B > A$, where $A = a s_n^{\text{eff}}$, $B = b s_n^{\text{eff}}$).

[6] In our numerical procedure, we can also use a slip-weakening law as that used by *Andrews* [1973, 1985]:

$$\tau = \begin{cases} \tau_u - (\tau_u - \tau_f)\dfrac{Du}{d_0}, & Du < d_0 \\ \tau_f, & Du \ge d_0 \end{cases} \qquad (5)$$

where τ_u is the upper yield stress, τ_f is the final, or kinetic, friction level, and d_0 is the characteristic slip-weakening distance.

[7] The characteristic length scale parameters of these two constitutive formulations are the slip-weakening distance d_0 and the parameter L: the former represents the slip required for traction to drop from τ_u to τ_f, the latter is the characteristic length controlling the evolution of the state variable. In a recent paper, *Cocco and Bizzarri* [2002] have investigated the slip-weakening behavior of rate- and state-constitutive laws and have shown that these two length

scale parameters are different. They propose a scaling law between d_0 and L, which states that their ratio is nearly 15. In the present study we aim to investigate in greater detail how the constitutive parameters control the slip-weakening behavior in the framework of RS dependent laws and to provide a theoretical explanation of numerical results.

[8] There is a lack of experimental evidence confirming that these RS constitutive laws can be used to represent fault friction at high slip rates. The constitutive laws defined in equations (3) and (4) have been derived from laboratory stick-slip experiments in which the slip velocities are in the range of few microns to 10 mm/s [*Mair and Marone*, 1999]. Laboratory experiments made by Ohnaka and coworkers [*Ohnaka et al.*, 1987; *Ohnaka and Shen*, 1999] show slip velocities within the preexisting crack up to 100 mm/s. Therefore we are confined to extrapolate the adopted constitutive laws at slip rates of the order of m/s as in real earthquake ruptures. This extrapolation is quite common in the literature (see, for instance, *Ide and Takeo* [1997], who used a SW law, or *Lapusta et al.* [2000] and *Guatteri et al.* [2001], who adopted RS laws). In this study we adopt the slowness and the slip constitutive formulations to model the breakdown process during the dynamic rupture propagation, therefore implicitly assuming that these laws are valid at relatively high slip rates.

3. Modeling a Spontaneous Rupture With Rate- and State-Dependent Friction Laws

3.1. Reference Model

[9] In this section, we present and discuss the main features of spontaneous crack propagation on a fault obeying a RS slowness law (equation (3)). We chose a reference set of parameters, which is typical of laboratory experiments: the medium surrounding the crack is linear elastic, homogeneous and Poissonian. The total fault length is equal to 20 m and, after initiation, the crack propagates symmetrically with respect to the nucleation point $x_1 = 0$. At the initial stage, the fault is in the steady state, except in the nucleation region, which is 3 m wide. Starting from the steady state, we simulate a spontaneous nucleation by choosing an initial configuration in which the nucleation stage is relatively short. This is justified by our purpose to simulate the breakdown process and the stress degradation at the crack tip during the dynamic propagation. The whole set of model parameters are listed in Table 1, and we refer to *Bizzarri et al.* [2001] for a detailed description of the adopted nucleation strategy for the simulations.

[10] Figure 1 shows the resulting total shear stress as a function of slip as well as the phase diagram (that is the traction as function of slip velocity) for a homogeneous fault where the spatial discretization is $\Delta x = 0.01$ m, and Δt is fixed from the Courant–Friedrichs–Levy (CFL) ratio w_{CFL}, defined as $v_S \Delta t/\Delta x$. We emphasize that, adopting a RS friction law, the dynamic traction clearly shows a slip–weakening behavior, as previously pointed out by *Okubo* [1989], *Dieterich and Kilgore* [1994] and *Bizzarri et al.* [2001]. We identify the slip–weakening distance on this plot, and according to *Cocco and Bizzarri* [2002], we named it an equivalent SW distance d_0^{eq}. In the following of this study, we estimate the slip–weakening distance from the traction versus slip curve by picking the slip value at the

Table 1. Reference Model Constitutive and Medium Parameters

Parameter	Value
$\lambda = \mu$	27 GPa
v_P	5196 m/s
v_S	3000 m/s
μ_*	0.56
a	0.012
b	0.016
σ_n^{eff}	100 MPa
L	1×10^{-5} m
$\Phi (x_1, t = 0)$ for x_1 $\in [-1.5$ m, 1.5 m]	$\Phi_{nucl} = 1 \times 10^{-4}$ s
$\Phi (x_1, t = 0)$ elsewhere	$\Phi^{ss} (v_{init})$
$\tau_0 \equiv \tau(x_1, t = 0)$	$\tau^{ss}(v_{init})$
Δx	0.01 m
Δt	$(0.95 \times 3^{1/2}) \Delta x/(2v_P) = 1.58 \times 10^{-6}$ s
$w_{CFL} = v_S \Delta t/\Delta x$	0.342

traction minimum. The simulation shown in Figure 1 represents a reference model for our investigations. Because we model here a homogeneous fault configuration, these ruptures are not confined; they do not arrest by themselves and propagate continuously. This is reasonable because we are not interested in the present paper to study the healing mechanisms. As pointed out by several authors [*Okubo*, 1989; *Gu and Wong*, 1991; *Guatteri et al.*, 2001; *Cocco and Bizzarri*, 2002], the equivalent SW distance d_0^{eq} is not equal to the L value adopted in the simulations. We will examine and discuss this difference more in detail in following sections.

3.2. Interpreting the Traction Evolution Within the Cohesive Zone

[11] In order to understand the evolution of dynamic traction within the cohesive zone and to identify the physical quantities controlling the SW behavior, we compare the time histories of total traction, slip velocity and state variable (Figure 2a) calculated for the same model parameters used in Figure 1 (i.e., the reference case) in the same fault position ($x_1 = 3.0$ m). By looking at Figures 2a and 2b it emerges that the resulting total dynamic traction reaches its peak value (the yield stress, τ_u^{eq}) earlier than slip velocity, and that the state variable evolves from its initial steady state value to a final one well before the other two. This first consideration allows us to suggest that it is the state variable that drives the slip acceleration and the traction drop during the weakening phase. This result is more evident in Figure 2b, where we compare the total dynamic traction to the logarithm of slip velocity and to the logarithm of state variable. We aim to discuss this topic in detail in the following of this section. We subdivide the time window shown in Figure 2 in five distinct stages, which comprise the duration of the whole breakdown process. The first stage (indicated as I in Figure 2) is characterized by a slight decrease of the state variable (which starts evolving from its steady state value) and a modest increase in traction; the slip velocity slightly increases from its initial value (v_{init}). Such an increase of traction is due to the contribution of those points that are already slipping (i.e., the dynamic load). During the phase II the shear traction continues to increase and reaches its peak value, while the slip velocity shows a fast increase only when the state variable decreases more rapidly. We denoted the time interval starting with the sharp slip velocity increase and lasting until the traction has
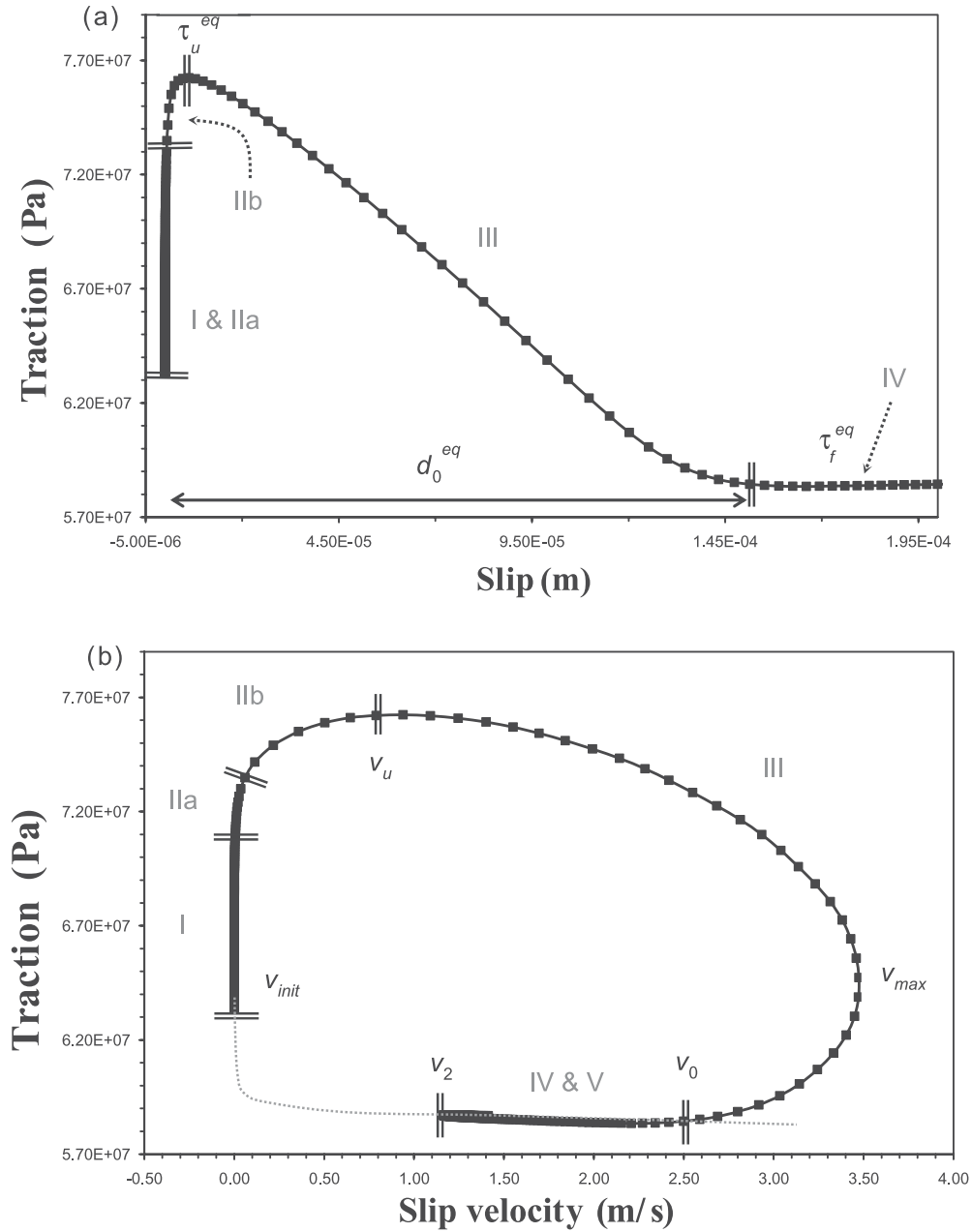
Figure 1. Total dynamic traction as a function of slip (a) and slip rate (b) (the latter is also named the phase diagram) in the fault position $x_1 = 3.0$ m for a propagating rupture obeying a slowness evolution law. Initial and constitutive parameters used for these calculations are listed in Table 1. We indicate with roman numbers different stages of the dynamic rupture process identified by particular values of traction and slip velocity (see text for a detailed description). The equivalent slip-weakening distance, the yield stress and the kinetic friction level are also shown in both the panels. The dotted line in Figure 1b shows the steady state friction.

Figure 2. (opposite) (a) Time histories of dynamic traction, slip velocity and the state variable computed for the same simulation shown in Figure 1. (b) Comparison between the temporal evolution of total traction and the logarithm of slip velocity ($\log(v)$) and state variable ($\log(\Phi)$). The roman numbers identify the different stages of the dynamic rupture process drawn in Figure 1 and described in the text. The slip velocity value reached when the traction is at its maximum value (τ_u^{eq}) is named v_u, while v_0 is the slip velocity at the end of the weakening process when the fault slip is d_0^{eq}. (c) Comparison between state variable time evolution during the phase IV obtained from the numerical simulation and the theoretical steady state curve ($\Phi^{ss}(v)$). This comparison confirms that during the stage IV the state variable is always at the steady state; v_2 is the final value of slip rate.

(a)

(b)

(c)
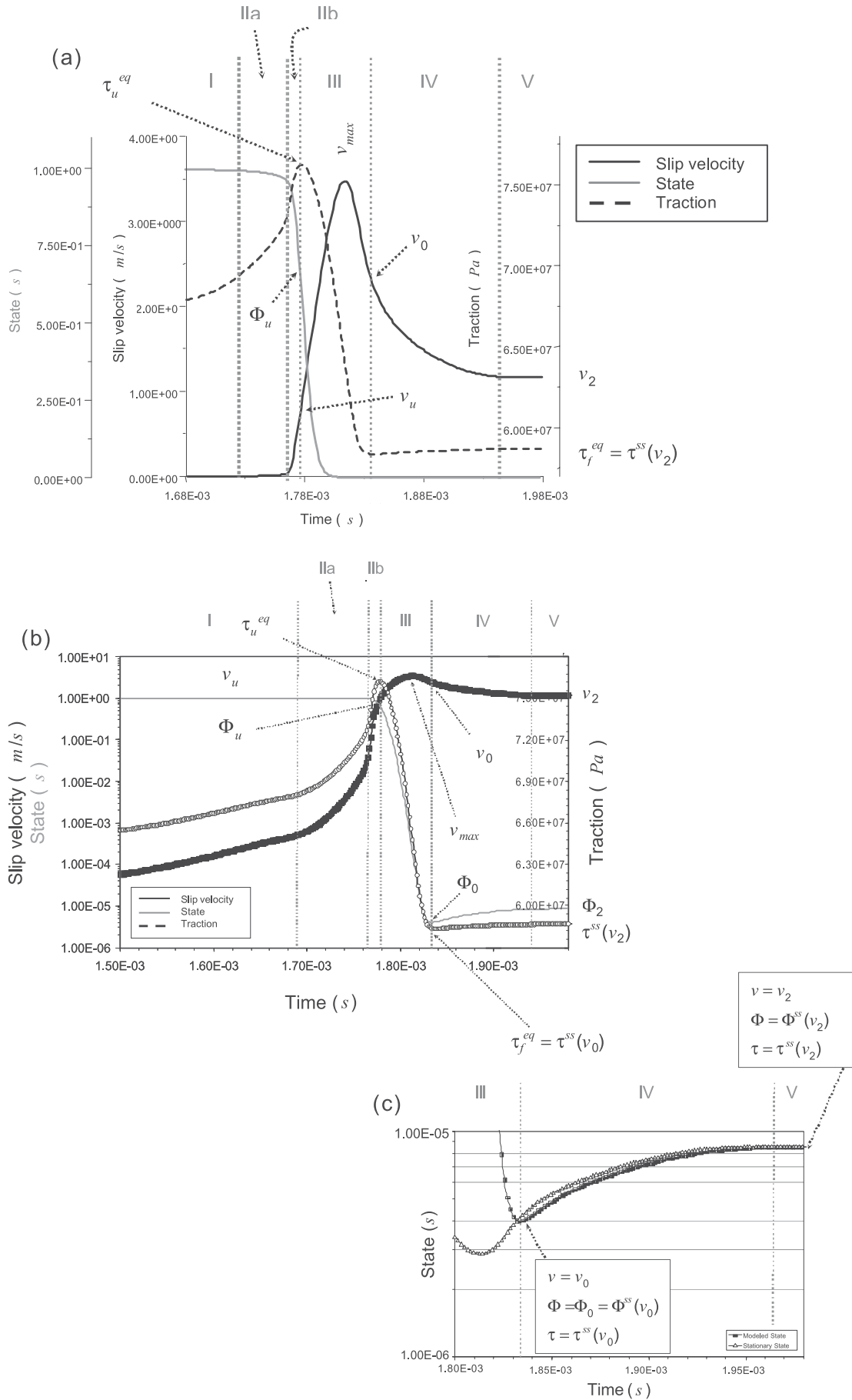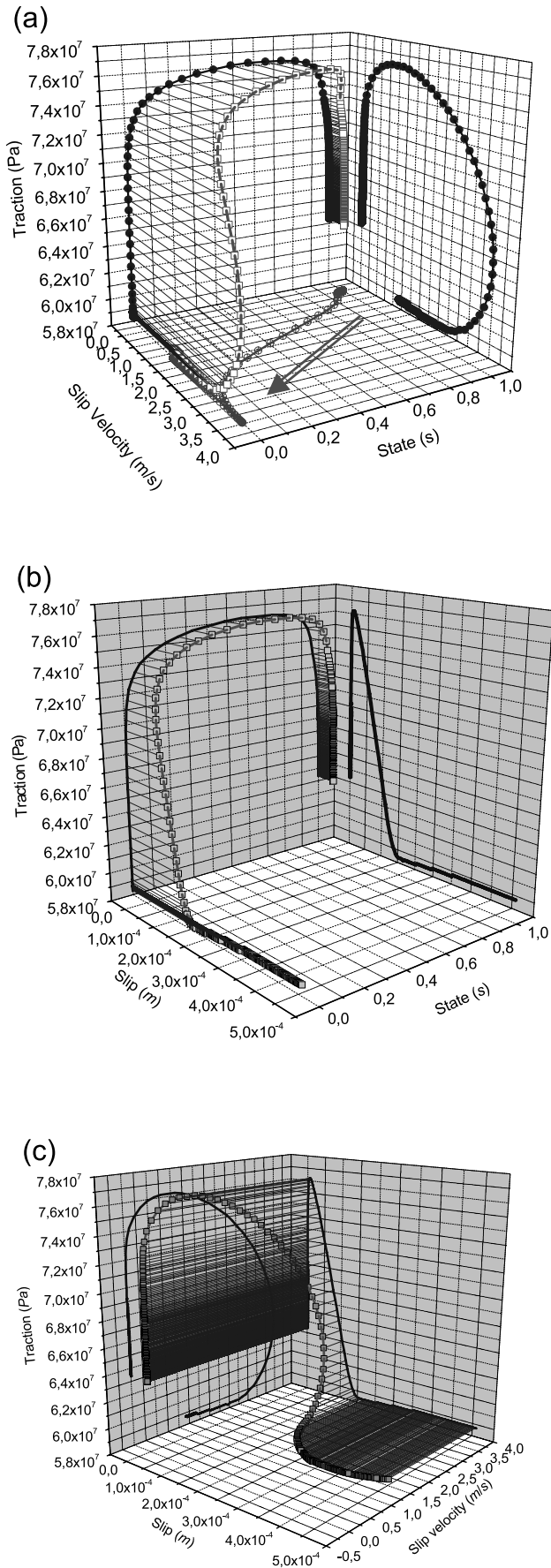
reached the yield stress value (τ_u^{eq}) as a phase IIb. We indicate with v_u and Φ_u the values of the slip velocity and state variable corresponding to the peak value of dynamic stress. We emphasize again that the total dynamic traction does not reach its maximum in correspondence to the peak of the slip velocity ($v_u < v_{max}$). This latter result is in agreement with the numerical results of *Olsen et al.* [2001] and *Mikumo et al.* [2003]. However, our results show that the maximum of slip velocity is not simultaneous with the minimum of dynamic traction. This result does not agree with those of *Mikumo et al.* [2003], as we will discuss in the following. Phases I and II represent the velocity–hardening phase depicted in Figure 1b.

[12] The slip-weakening phase begins when the total dynamic traction has reached τ_u^{eq}; we named this stage (whose duration defines the breakdown zone time T_b) as phase III, during which the state variable drops to its minimum value Φ_0 (see Figure 2c). Most of the state variable evolution occurs during this short stage (phase III in Figures 1 and 2) corresponding to weakening phase, emphasizing that this temporal variation is extremely fast. During the weakening phase (III) the slip velocity first rapidly increases, reaches its maximum value (v_{max}), and therefore decreases. We named v_0 the slip velocity value at the end of the weakening phase (III) when the traction is at its minimum and the slip is equal to d_0^{eq}. At this point, and for the subsequent phase IV, the state variable is already close to its steady state curve $\Phi^{ss}(v)$: this is clear by looking at the log–linear plot in Figure 2c, where we have represented a zoom of the state variable time history plotted in Figure 2a superimposed to the stationary state $\Phi^{ss}(v) = L/v$. Figure 2c confirms that when the SW phase (stage III) is ended (the traction drop is concluded), the state variable is at the steady state. At this time the friction is $\mu(v_0, \Phi^{ss}(v_0))\sigma_n^{eff} = \mu^{ss}(v_0)\sigma_n^{eff}$. This value corresponds to the kinetic traction τ_f^{eq} in the SW model, as we will derive in a following section. This phase IV is characterized by a slip velocity decrease down to the final level v_2, the state remain in its steady state and therefore the friction is $\mu^{ss}(v_2)\sigma_n^{eff}$. The slip velocity maintains its final value (v_2 in our simulations) if no healing of slip occurs [see *Perrin et al.*, 1995].

[13] These considerations can be easily summarized by looking at the 3–D phase trajectories shown in Figure 3: the state variable drives the slip acceleration (Figure 3a) and the traction drop during the weakening phase (Figure 3b). The SW begins when the state variable is already evolving (see Figures 2a and 3b) and the accelerating phase is already started (see Figures 2b and 3c). Nevertheless, a relevant fraction of the state is lost during the weakening phase (see Figures 2b and 3a). Several recent papers [*Olsen et al.*, 2001; *Mikumo et al.*, 2003] have shown that, adopting a SW

Figure 3. (opposite) Three-dimensional trajectories representing the total dynamic traction as a function of (a) slip velocity and state variable, (b) slip and state, and (c) slip and slip velocity. These plots refer to the same simulations and to the same fault position used for previous figures. The arrow in Figure 3a has been drawn to point out the increase of slip velocity driven by the state variable evolution. Figure 3b clearly shows that SW begins when the state variable is already evolving from its initial (steady state) value.

constitutive law, the slip velocity reaches its peak value when the dynamic traction is at its minimum value (i.e., the kinetic friction) and the slip is equal to d_0. Our simulations clearly show that, adopting rate- and state-dependent laws, peak slip velocity is not simultaneous with the minimum traction.

[14] Several stimulating questions arise from these results: if the traction drop during the weakening phase is controlled by the state variable, does it mean that the SW behavior and the breakdown process depends on the properties of the contacts on the surface within the cohesive zone? And how much the analytical expression chosen for the evolution law controls the SW behavior? We aim to discuss these questions in the present study. To this goal we must investigate the temporal evolution of slip, slip velocity and dynamic traction within the cohesive zone (as done in Figure 2). This requires discussing the available resolution and the stability conditions before to present the results of numerous simulations performed with different constitutive parameters and initial conditions. We face this problem in the following section.

4. Testing the Resolution of the Cohesive Zone

[15] The investigation of the temporal evolution of the physical quantities that characterize the breakdown process requires an accurate control of the stability of the solutions and the available resolution of the cohesive zone, which are needed to model the slip acceleration. In order to solve the elastodynamic equation with numerical algorithms, such as the finite difference approach used in this study, this control is usually done by verifying a precise set of relations (see Appendix A). *Bizzarri et al.* [2001] discussed these relations in detail. They are used to check the capability of the numerical simulation to resolve the temporal dynamic evolution of the rupture process and to satisfy few spatial discretization requirements. However, even if all the necessary conditions for convergence and stability are satisfied, this does not guarantees to have enough resolution to follow the state variable evolution and the fast slip acceleration. We have shown in Figure 2 that slip velocity reaches its peak value in an extremely short time, and therefore the adopted spatial and temporal discretization have to be appropriately selected.

[16] In order to find the most convenient choice of Δx and Δt, we repeat the simulation presented in Figure 1 by choosing different spatial and temporal discretizations. In a first analysis, we have selected different spatial grid sizes Δx and, because we do not change the Courant–Friedrichs–Levy (CFL) ratio w_{CFL} ($w_{CFL} = v_S \Delta t/\Delta x$), the temporal step size Δt is varied consequently. We show in Figure 4 the traction versus slip (Figure 4a) and the slip velocity time history (Figure 4b) for four different cases, for which the discretization changes, but all the other parameters and the fault position ($x_1 = 3.0$ m) remain the same used before and listed in Table 1. The slip-weakening curves plotted in Figure 4a show that the increase in Δx (and consequently of Δt) modifies both the weakening rate and the equivalent slip-weakening distance. When we adopt a smaller Δx the decrease of traction with increasing slip becomes close to a linear decay; on the contrary, with a larger spatial and temporal discretization, the simulations

exhibit a more evident roll-off in correspondence of the maximum shear traction (τ_u^{eq}). Therefore the estimate of the equivalent characteristic distance (d_0^{eq}) can be biased by the adopted spatial and temporal discretization; for the case considered here Δx must be smaller than 0.01 m to properly evaluate d_0^{eq}. Moreover, Figure 4b shows that the peak of slip velocity is well resolved only when Δx is smaller than 0.01 m. It is important to note that by changing the temporal step we also change the local stiffness k, that is expressed as the inverse of the local compliance C (see Appendix A). Because the ratio k/k_{crit} is known to control the stability of the fault frictional behavior [*Scholz*, 1990; *Dieterich*, 1992], as Δt decreases the local stiffness increases and the fault begins to be more stable (and, in fact, the dynamic instability occurs later, see Figure 4b). This might explain the change in the shape of the SW curve, which we observe also when the convergence, continuity, and stability criteria are strictly verified.

[17] In order to investigate the importance of the coupling between spatial and temporal steps, we have simultaneously varied Δx and the w_{CFL} ratio, which allows us to maintain Δt constant (and therefore to fix the fault stiffness); w_{CFL} is known to control the convergence of numerical methods, both for BIE and FD approaches: *Fukuyama and Madariaga* [1998], by using a 3-D BIE code with a SW equation, noted that w_{CFL} is responsible for fluctuations and oscillations in slip velocity and rupture velocity. The results of our 2-D simulations are shown in Figure 5. While the SW curve, and the d_0^{eq} are completely independent on the CFL ratio (Figure 5a), as expected because the fault stiffness is constant in this case, the phase diagram strongly exhibit a dependence on w_{CFL}. In particular, we emphasize the different values of peak slip velocity, which increases as w_{CFL} decreases (i.e., as Δx increases).

[18] We summarize in the Appendix A the conditions that must be satisfied to have enough resolution of the cohesive zone. We use them to select the appropriate time and spatial steps that allow us to resolve the traction evolution and the slip velocity time history. We emphasize that, when the spatial and temporal discretization are appropriately selected, the traction drop for increasing slip is nearly constant, which results in a linear decay with a constant weakening rate. We remark that the resolution of the fast state variable evolution (see Figure 2a) guarantees to appropriately model the fast slip acceleration. This later result has important implications for the actual capability to model radiated waveforms with dynamic consistent source models, as well as to use ground motions to constrain fault constitutive parameters [see *Guatteri and Spudich*, 2000; *Guatteri et al.*, 2001].

5. A Scaling Law for the Two Characteristic Length Scale Parameters

[19] In this section we discuss the dependence on the parameter L of the equivalent characteristic distance d_0^{eq} inferred from numerical simulations. The constitutive parameters adopted for the simulations are those used in the previous figures and listed in Table 1, and only the parameter L is varied. We adopt an appropriately selected spatial (and temporal) discretization, which allows us to model the dynamic traction evolution for all the cases
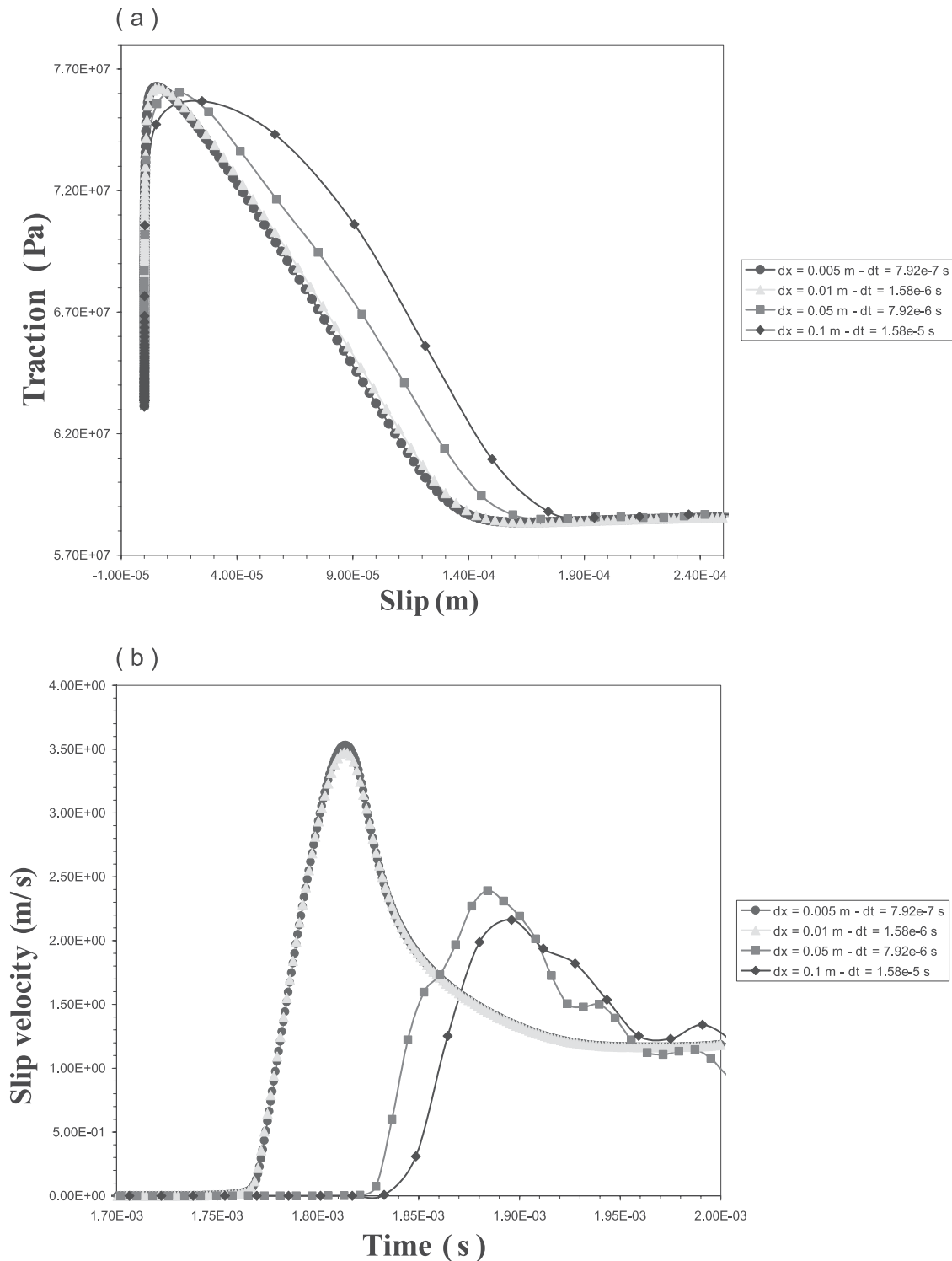
(a)

(b)

Figure 4. (a) Slip-weakening curves and (b) slip velocity time histories computed for different spatial and temporal discretization (Δx and Δt, respectively). The temporal grid spacing Δt is varied because we maintain constant the Courant-Friedrichs-Levy ratio (w_{CFL}). This implies that the local fault stiffness k is different among the different simulations presented here.

considered here: we assume $\Delta x = 0.005$ m and the calculations are performed with 1401 points in space (x_1) and 5000 points in time (t). In Figure 6, we show five different SW curves obtained with different L, which shows quite different traction behaviors. This figure suggests a direct

dependence of d_0^{eq} on L and a weak inverse dependence of τ_u^{eq} on L, implying that the weakening rate decreases for increasing L. We note however that, when L is large enough to change the critical stiffness of the system (as in the two simulations presented here having the largest L values), the
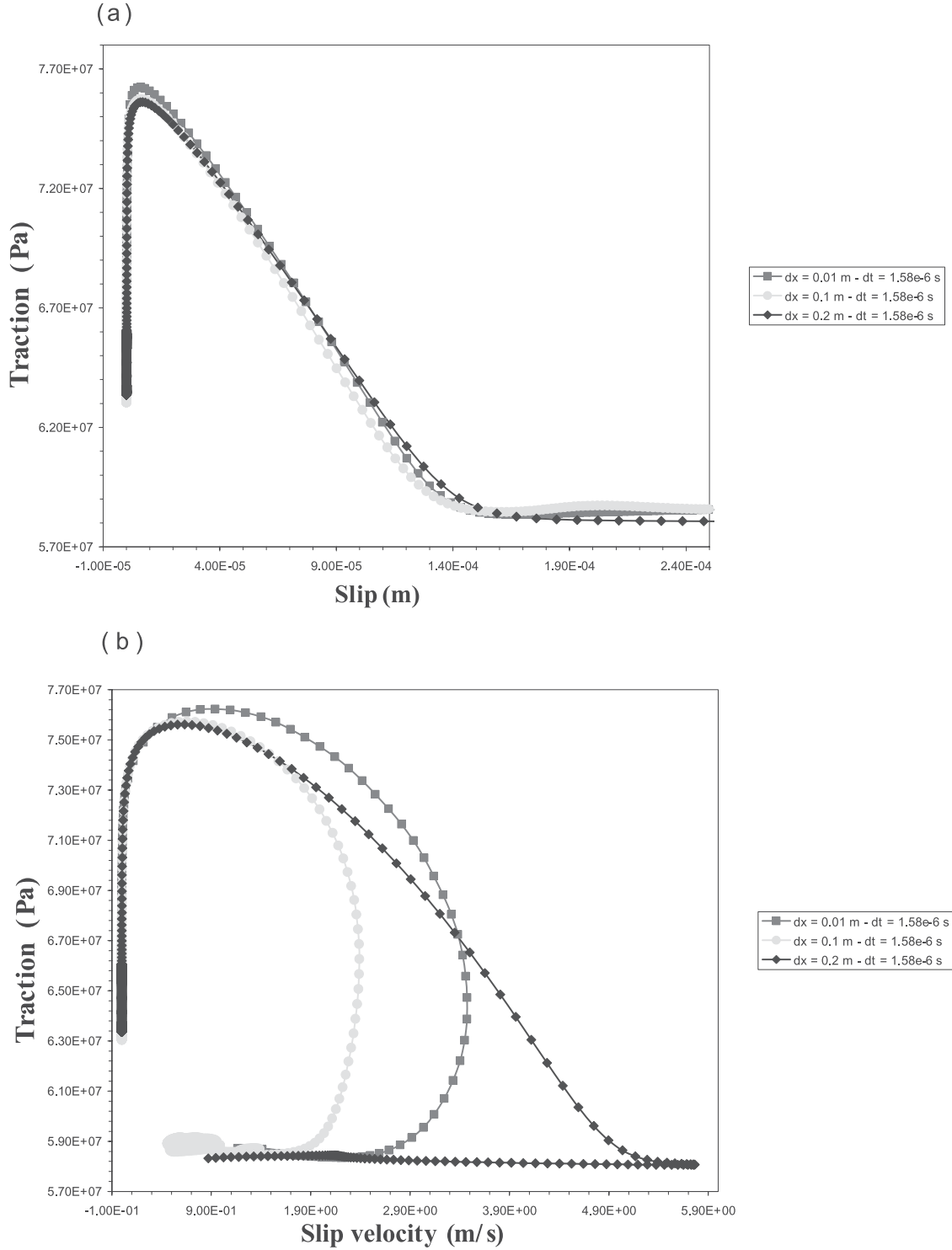
(a)

(b)

Figure 5. (a) Slip-weakening curve and (b) phase diagram resulting from simulations performed with different spatial grid size and constant time steps. The Courant-Friedrichs-Levy ratio, w_{CFL}, is now different, which implies that the local fault stiffness k is now constant among all the simulations presented here.

dependence of the yield stress on L is more evident. It is important to point out that when L increases the fault undergoes to the instability more slowly, because the evolution of the state variable is slow. Because the critical patch size (l_c), which in turn controls the rupture nucle-

ation, is analytically expressed as $\eta\mu L/(b - a)\,\sigma_n^{eff}$ (η being a geometrical, dimensionless, numerical parameter), when L increases, l_c increases too, and therefore the fault had to spend a longer time and had to produce a larger slip to reach an extension equal to l_c.
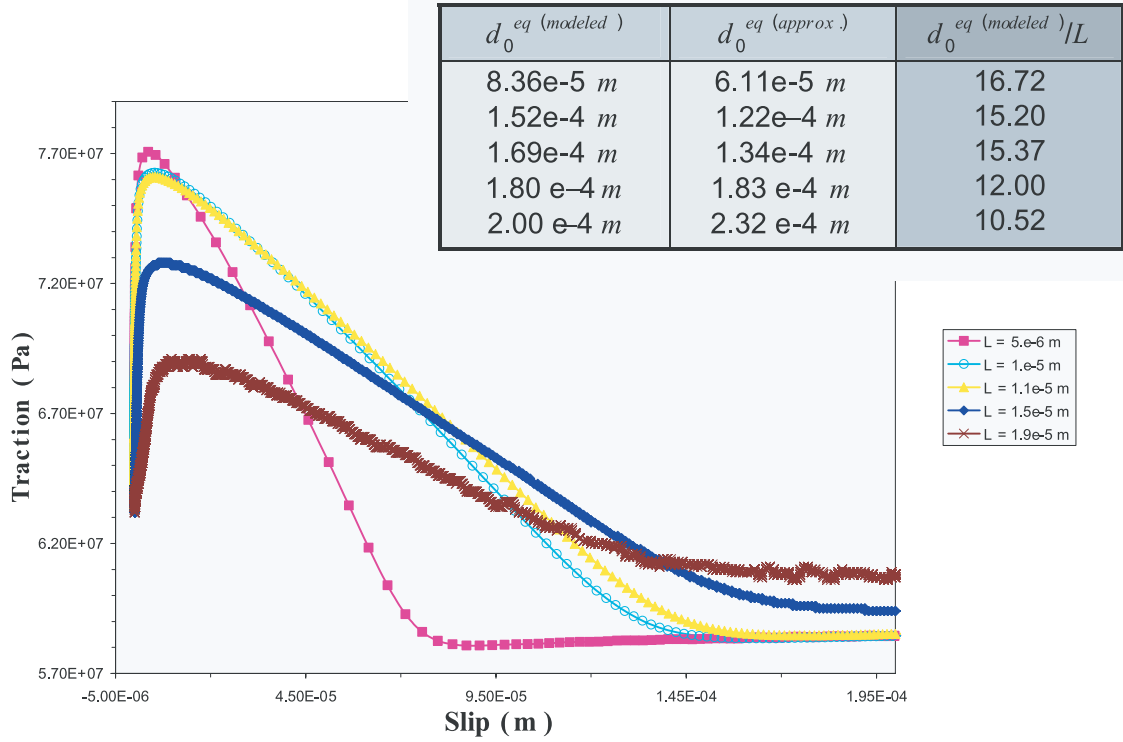
d_0^{eq} (modeled)	d_0^{eq} (approx.)	d_0^{eq} (modeled)/L
8.36e-5 m	6.11e-5 m	16.72
1.52e-4 m	1.22e–4 m	15.20
1.69e-4 m	1.34e-4 m	15.37
1.80 e–4 m	1.83 e-4 m	12.00
2.00 e-4 m	2.32 e-4 m	10.52

Legend:
- L = 5.e-6 m
- L = 1.e-5 m
- L = 1.1e-5 m
- L = 1.5e-5 m
- L = 1.9e-5 m

Figure 6. SW curves calculated for different length scale parameters L. All the model parameters are the same used in Figures 1 and 2, but we modify the spatial discretization in order to correctly resolve the cohesive zone (see Appendix A for details), this is required for the simulations with small L (we use $\Delta x = 0.005$ m). In the box are showed the modeled and the approximated values of d_0^{eq} (see text for the details).

[20] The top right insert in Figure 6 shows the d_0^{eq} values resulting from the simulations and the ratio d_0^{eq}/L. We now derive an analytical relationship between these two length scale parameters (d_0^{eq} and L) accordingly to the results of *Cocco and Bizzarri* [2002]. To this aim, we rewrite the evolution equation (3b) (i.e., the slowness law) in the following way:

$$\frac{d}{du}\Phi = \frac{1}{v} - \frac{\Phi}{L}. \tag{6}$$

During the stage III (see Figure 2a), we have that $u \leq d_0^{eq}$ but v is large enough to allow the term $1/v$ in equation (6) to be neglected. Because the condition $1/v \ll \Phi/L$ is always satisfied within the cohesive zone in all our simulations, the integration of the approximated evolution equation yields

$$\Phi(u) \cong \Phi(u = 0)e^{-u/L} = \Phi_{\text{init}}e^{-u/L} \tag{7}$$

where Φ_{init} is the initial value of the state variable. We have defined in Figure 2a that when the slip equals d_0^{eq} the slip velocity is v_0 and the state variable is at the steady state, $\Phi^{ss}(v_0)$. Thus, from equation (7) we have

$$\Phi_{\text{init}}e^{-\frac{d_0^{eq}}{L}} = \frac{L}{v_0}, \tag{8}$$

which yields

$$d_0^{eq} \cong L \ln\left(\frac{\Phi_{\text{init}}v_0}{L}\right). \tag{9}$$

As in the work by *Cocco and Bizzarri* [2002], we assume in the following of this paper that the initial value of state variable is a steady state value: $\Phi_{\text{init}} = \Phi^{ss}(v_{\text{init}}) = L/v_{\text{init}}$. For this particular initial condition (i.e., steady state) equation (9) becomes

$$d_0^{eq} \cong L \ln\left(\frac{v_o}{v_{\text{init}}}\right), \tag{10}$$

which corresponds to the relation previously derived by *Cocco and Bizzarri* [2002]. Equation (9) represents a more general scaling law than equation (10). These two equations show that the equivalent slip-weakening distance d_0^{eq} depends on L and the initial state, which at the steady state is identified by the initial velocity. In order to estimate the theoretical value of the equivalent slip-weakening distance through equation (10), we have to evaluate the slip velocity v_0 that is a priori unknown in the framework of rate- and state-constitutive formulation. We have derived an approximated expression in Appendix B that relates the slip velocity v_0 to the constitutive parameters, using the shear impedance relation [*Scholz*, 1990]. By means of this approximation and of equation (10) we have calculated the theoretically derived values of the equivalent SW distance for the different parameters used in Figure 6, and we have inserted these values in the panel of that figure. We will discuss in a following section the problems related to the lack of knowledge of the slip velocity values associated with the different stages of the breakdown process represented in Figure 2.

[21] The important result emerging from these numerical simulations is that the scaling law between d_0^{eq} and L is very close to a linear relation and the proportionality ratio is nearly 15, only when the initial state is a steady state and equation (10) holds. This is in agreement with the results of *Cocco and Bizzarri* [2002]. However, for a more general case with an arbitrary initial value of the state variable equation (9) holds; in this case the proportionality factor between d_0^{eq} and L can be much larger (for instance, 50, for values of the initial state variable of 100 years). We also note that, as L increases, τ_u^{eq} decreases and, on the contrary, τ_f^{eq} increases. We will further discuss these results in the next sections. We point out that, the velocity-hardening effects (phases I and II in Figures 1 and 2) are always present independently of the adopted constitutive parameters, but the slip-hardening distance (i.e., the amount of slip necessary to dynamic traction to reach the equivalent upper yield stress) is negligible unless the value of the parameter L becomes very large (see Figure 6). The former result is intrinsic in the RS formulation: the rate dependence implicitly involves the existence of both velocity-hardening and weakening effects [see *Bizzarri et al.*, 2001]. Slip-weakening is also a peculiarity of RS laws [see *Guatteri et al.*, 2001; *Cocco and Bizzarri*, 2002], but the slip-hardening effects depend on the evolution of the state variable, which in this formulation is controlled by the value of the constitutive parameter L.

6. Dependence on the Constitutive Parameters *a* and *b*

[22] We discuss the results of numerical simulations performed by using different values of the constitutive parameters a and b, but keeping L constant. We choose different a and b values, within the velocity-weakening frictional regime, ranging between 0.008 and 0.0125 and between 0.0155 and 0.020, respectively. The other model parameters are constant and are listed in Table 1; we have used 701 grid points in space (x_1) and 10000 in time (t). All the plots discussed in the following are referred to the fault position $x_1 = 3.0$ m, as in the previous calculations. In Figure 7 we show the results of five simulations obtained using different a values. The behavior of total shear traction as function of displacement (Figure 7a) shows that the upper yield stress τ_u^{eq} and the equivalent characteristic distance d_0^{eq} depend on the a parameter: when a increases, both τ_u^{eq} and d_0^{eq} decreases. Moreover, Figure 7b shows that when a increases the peak slip velocity decreases. This is due to the direct effect of friction, which reduces peak slip velocity and yield stress. These results are in agreement with those obtained by *He et al.* [2003], who analyzed stick-slip instabilities simulated through a spring slider dynamic system. According to their conclusions, v_{peak} is reduced when the yield stress decreases because the stored available elastic strain energy driving the stress drop is lower. We observe that the weakening rate does not change with the adopted value of the a parameter, as clearly shown in Figure 7a.

[23] Figure 8 shows the results of similar calculations, but adopting different b values. We note a dependence on the b parameter of both the yield stress and the equivalent characteristic distance: they increase for increasing b, while the weakening rate is nearly constant in all the cases considered here. The peak slip velocity increases with the adopted b value, in agreement with *He et al.* [2003]. Figure 9 points out the effect of different $b - a$. Symbols and colors show the SW curves for the same $(b - a)$ value: open symbols indicate the curve resulting from the reference a value ($a = 0.012$) with different b, while solid symbols refer to different a values with the same reference b value ($b = 0.016$). Figure 9 emphasizes that the kinetic friction (τ_f^{eq}) only depends on the difference $b - a$, and not on the absolute values of a and b. On the contrary, our simulations show that the maximum yield stress depends on the individual adopted values of a and b (Figure 9a) and the same behavior is found for the peak slip velocity (Figure 9b). As expected, a smaller value of the difference $(b - a)$ implies a smaller stress drop [see *Boatwright and Cocco*, 1996]. We observe that, for the same $b - a$, the simulations with bigger b determine a larger value of the yield stress τ_u^{eq} and of the peak slip velocity. This result seems not to be consistent with the conclusions of *He et al.* [2003]. This discrepancy can be partially explained considering that we assume a steady state as initial condition. Therefore, changing a or b we vary the starting stress value, which is not the same in all the simulations presented in Figures 7, 8, and 9. However, also accounting for the different initial stress, the equivalent strength excess $(\tau_u^{eq} - \tau_0)$ depends on the individual values of constitutive parameters, because peak slip velocity also depends on these parameters.

7. Theoretical Interpretation

[24] We aim to propose analytical relations to express the SW parameters (yield and kinetic stress values) as a function of the input constitutive parameters, to be associated with the scaling law between the two length scale parameters, expressed in equations (9) and (10). We derive an expression of the dynamic friction which is valid when the slip acceleration phase is already started and equation (7) holds. By inserting equation (7) in equation (3a), and neglecting the +1 term in the argument of logarithms, we can express fault friction as a function of slip velocity and slip:

$$\tau = \left[\mu_* + a \ln\left(\frac{v}{v_*}\right) + b \ln\left(\frac{v_*}{v_{init}}\right) - b\frac{u}{L}\right]\sigma_n^{eff} \qquad (11)$$

Equation (11) expresses the governing equation for friction during the breakdown process as a function of slip and slip velocity and it is analogous to equation (3a) when the state variable is expressed by equation (7). This equation allows us to derive the analytical expression for the kinetic friction level: in fact, when the slip is equal to the d_0^{eq} and the slip velocity is v_0 we have:

$$\tau = \left[\mu_* + a \ln\left(\frac{v_o}{v_*}\right) + b \ln\left(\frac{v_*}{v_{init}}\right) - b\frac{d_o^{eq}}{L}\right]\sigma_n^{eff}; \qquad (12)$$

by substituting equation (10) in (12) and with simple algebra we can derive the following relation for the kinetic stress (τ_f^{eq}):

$$\tau_f^{eq} = \left[\mu_* + (b - a) + ln\left(\frac{v_*}{v_o}\right)\right]\sigma_n^{eff}. \qquad (13)$$

(a)

(b)

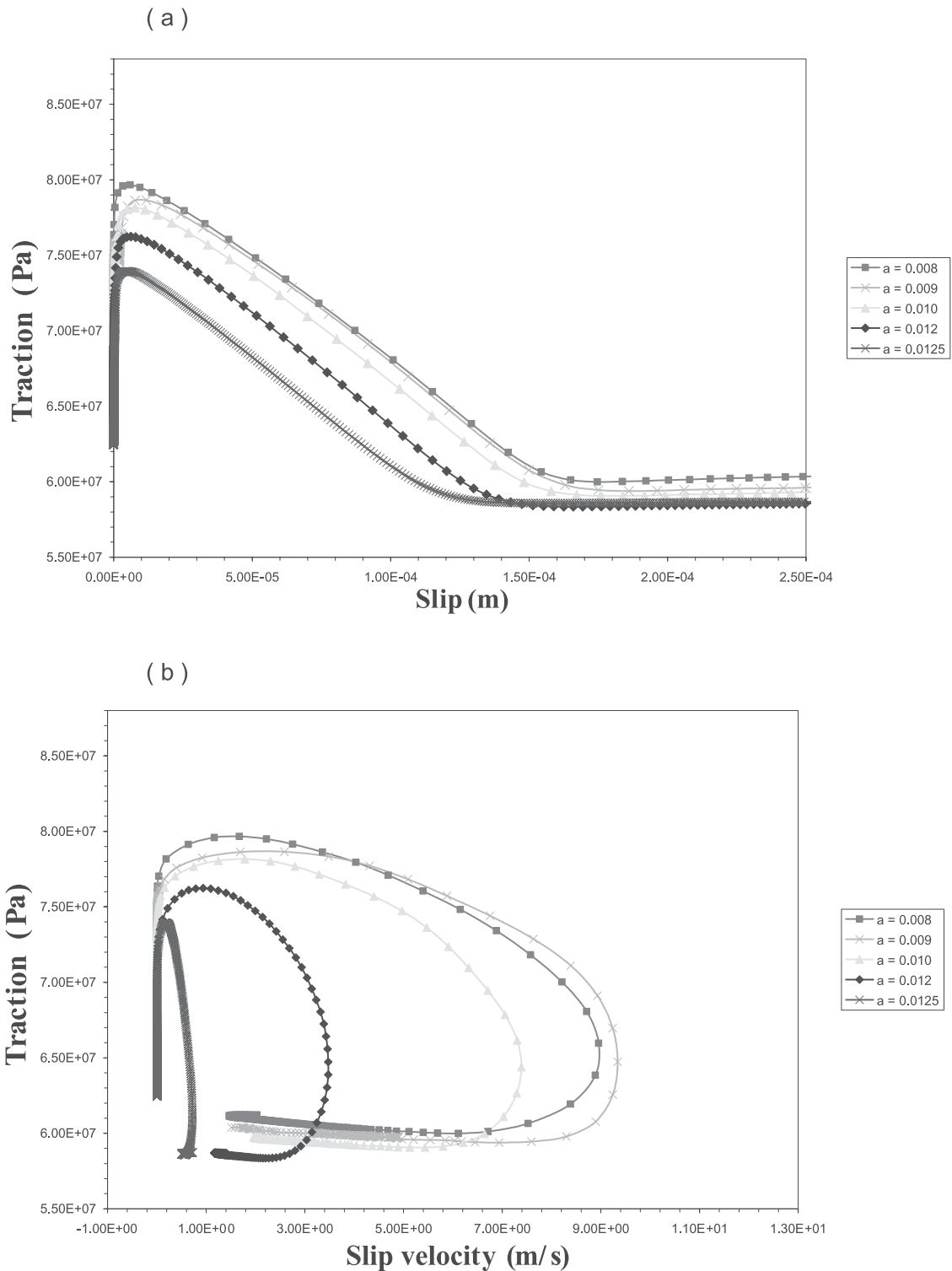**Figure 7.** Dependence on the *a* parameter: (a) and the SW curve and (b) the phase diagram calculated with different values of *a*, leaving unchanged all the others. The initial parameters are the same used in previous calculations and the plots are computed at $x_1 = 3.0$ m. The reference case (plotted in Figure 1) is included in this figure (solid curve with squares).

[25] It is interesting to observe that this expression coincides with the steady state value of fault friction for $v = v_0$ ($\tau_f^{eq} = \tau^{ss}(v_0)$). This is a further theoretical corroboration of the numerical results plotted in Figure 2c. Equation (13) confirms our interpretation of the numerical simulations

(presented in Figures 7, 8, and 9) that the kinetic friction only depends on the difference $b - a$ (it has to be noted here that also v_0 depends only on the difference $(b - a)$, see equation (B4)).

[26] The derivation of the analytical expression for the yield stress is slightly more complex. Figures 2 and 3
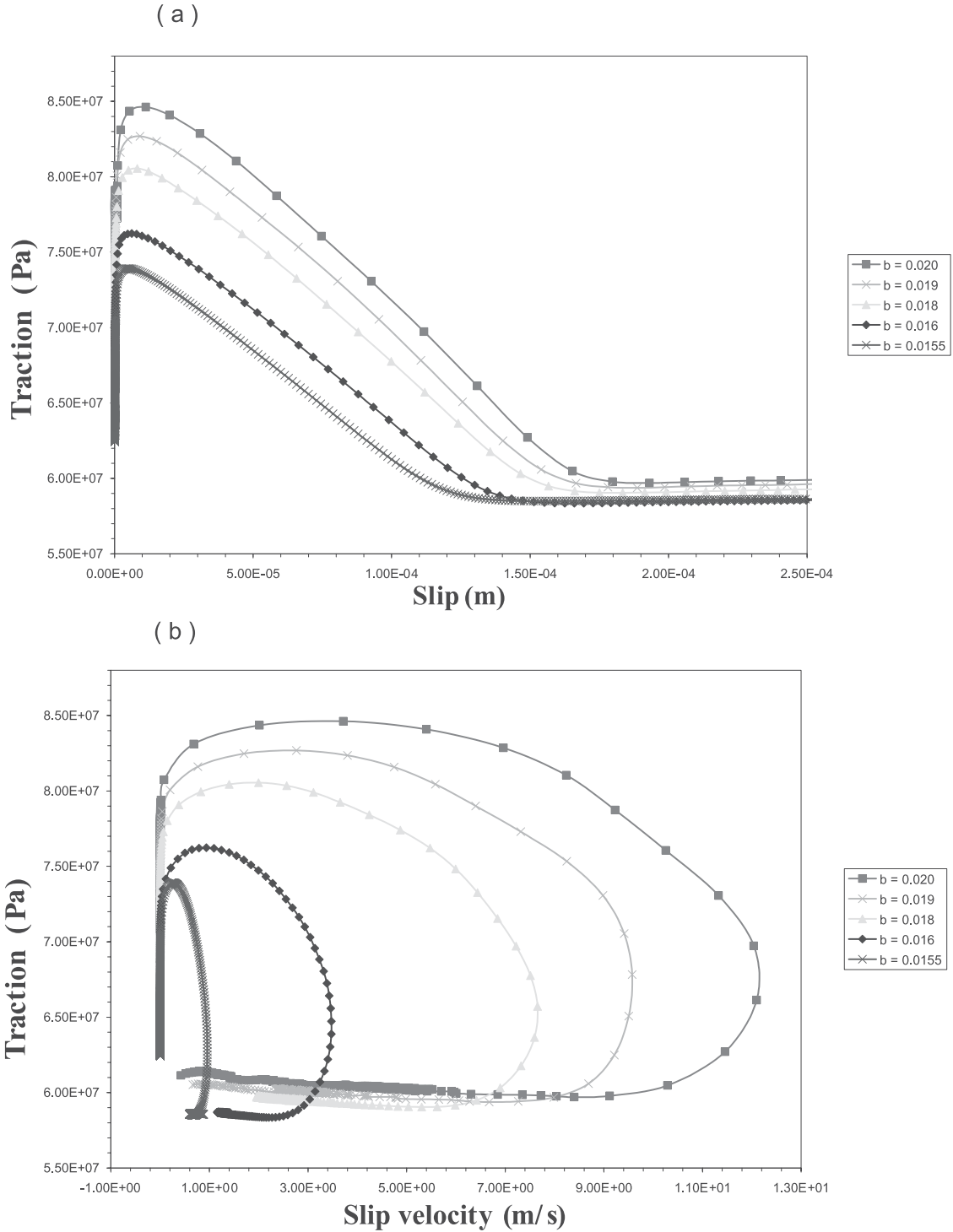
(a)

(b)

Figure 8.   Same as Figure 7 but using different values of the b parameter.

clearly show that when the total dynamic traction increases to the peak yield stress the state variable is evolving and driving the slip acceleration. Fault friction (i.e., the total dynamic traction) reaches its peak value (i.e., the yield stress) well before than slip velocity. In other words, the traction behavior within the cohesive zone is associated with the state variable evolution toward its final steady state value. We therefore rewrite the governing equation for fault friction as defined in equation (3a),

neglecting the $+ 1$ term in the arguments of logarithms, as follows:

$$\tau_u^{eq} = \left[\mu_* + a \ln\left(\frac{v_u}{v_*}\right) + b \ln\left(\frac{\Phi_u v_*}{L}\right) \right] \sigma_n^{\text{eff}}, \qquad (14)$$

denoting with v_u and Φ_u the slip velocity and the state variable when traction is at the yield stress (see Figures 2a and 2b). It has to be noted that the values of slip velocity
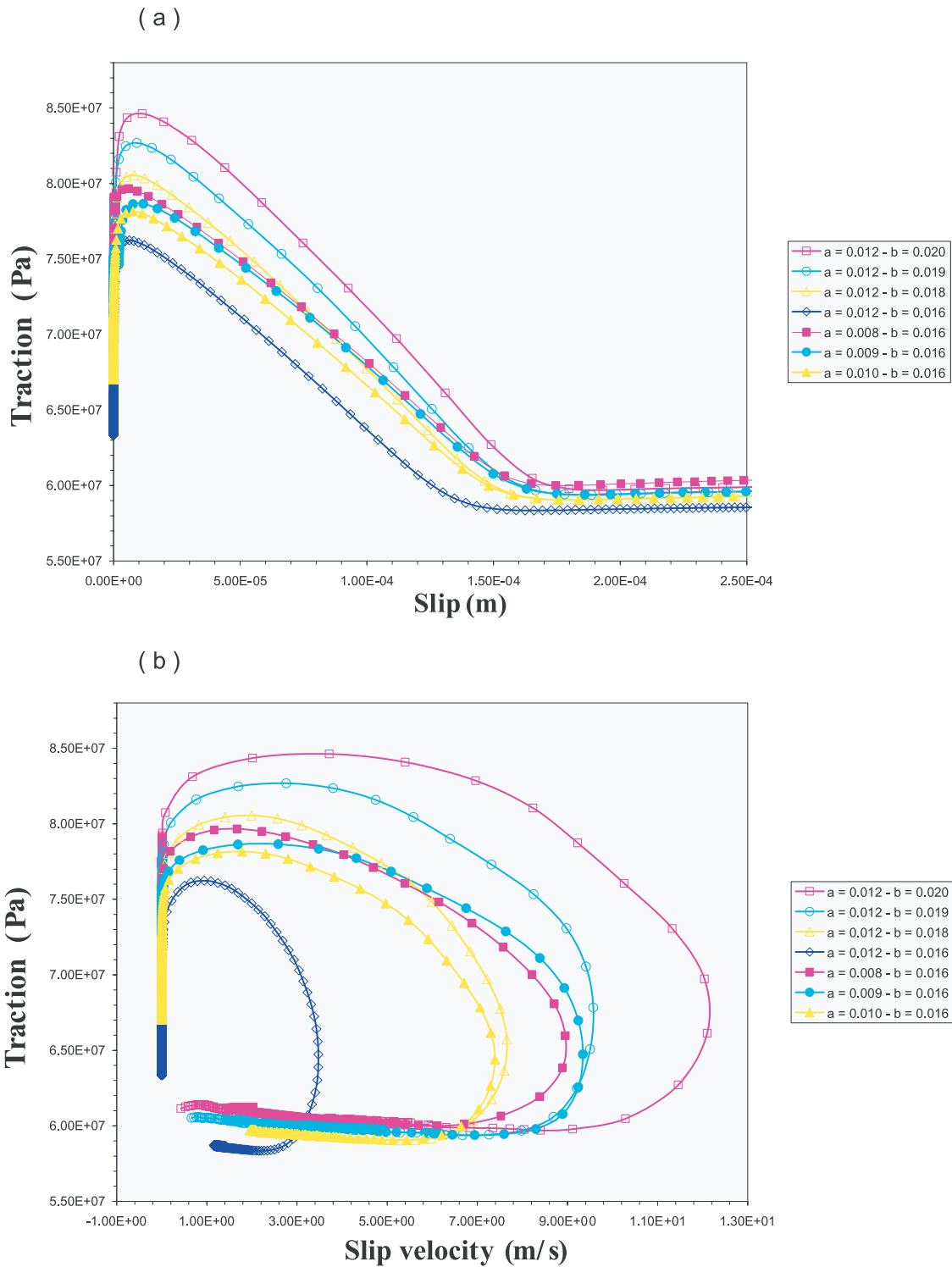
(a)

(b)

Figure 9. Traction dependence on the difference $(b - a)$: colors correspond to the same difference $(b - a)$. Open symbols refer to fixed a value $(a = 0.012)$ and different b; solid symbols refer to different a values and a fixed b $(b = 0.016)$.

(v_u) and state variable (Φ_u) at the peak stress (which appears in equation (14)) are unknown a priori, as well as the slip velocity v_0 that appears in equations (10) and (13). We have listed in Table 2 the values of slip-weakening parameters evaluated through the analytical relations (10), (13), and (14), by approximating v_u, Φ_u, and v_0 with the empirical relations discussed in Appendix B. Table 2 allows the comparison between analytical values of SW parameters and those resulting from numerical simulations. Each line in Table 2 corresponds to different a and b parameters but constant $(b - a)$. Equations (13) and (14) represent from an analytical point of view the concept that

Table 2. Comparison Between Numerically Modeled and Theoretically Approximated Values[a]

Different a $b = 0.016$	Different b $a = 0.012$	$d_0^{\text{eq(mod)}}$, m	$d_0^{\text{eq(app)}}$, m	$\tau_u^{\text{eq(mod)}}$, Pa	$\tau_u^{\text{eq(app)}}$, Pa	$\tau_f^{\text{eq(mod)}}$, Pa	$\tau_f^{\text{eq(app)}}$, Pa
	0.020	1.80E-04	1.30E-04	8.46E+07	8.29E+07	6.08E+07	6.08E+07
0.008		1.65E-04	1.30E-04	7.96E+07	7.86E+07	6.01E+07	6.01E+07
	0.019	1.78E-04	1.28E-04	8.27E+07	8.10E+07	5.99E+07	5.99E+07
0.009		1.63E-04	1.28E-04	7.87E+07	7.78E+07	5.90E+07	5.90E+07
	0.018	1.66E-04	1.27E-04	8.06E+07	7.91E+07	5.96E+07	5.96E+07
0.010		1.58E-04	1.27E-04	7.82E+07	7.70E+07	5.96E+07	5.96E+07
0.012	0.016	1.51E-04	1.22E-04	7.62E+07	7.51E+07	5.87E+07	5.87E+07

[a] Read 1.80E-04 as 1.80×10^{-4}.

the traction behavior within the cohesive zone cannot be assigned a priori in the framework of RS constitutive formulation. In our opinion, this might represent a limitation in using rate- and state-dependent constitutive laws in dynamic model of earthquake rupture propagation during a single earthquake. For such purposes, the adoption of a classical slip-weakening law (as defined in equation (5)) is numerically more convenient, because it allows prescribing the traction evolution and therefore to control the fracture energy absorbed at the crack tip. In the framework of a RS formulation, the slip velocity values controlling the traction evolution within the cohesive zone are not specified or assigned (see equations (10), (13), and (14)): therefore the yield stress, the kinetic friction and the characteristic slip-weakening distance cannot be prescribed a priori. These parameters, which are commonly assigned as input values in SW models, depend in the RS formalism on the constitutive parameters and initial conditions.

[27] Equation (10) shows a dependence of the equivalent slip-weakening distance on the initial slip velocity v_{init}. As discussed before, this parameter influences the initial value of the state variable, which in our simulations starts from a steady state $\Phi^{ss}(v_{\text{init}}) = L/v_{\text{init}}$, and consequently the initial stress value. This means that the (equivalent) strength parameter S (as defined by *Das and Aki* [1977a, 1977b] [see also *Bizzarri et al.*, 2001]) changes varying the initial slip velocity. This is well represented in Figure 10, where we plot the SW curve and the phase diagram for different values of the initial slip velocity, which shows that the fault response varies by changing v_{init}. This observation corroborates our interpretation that the evolution of the state variable from its initial value drives slip acceleration and the unstable response (i.e., the weakening effects). In this study we use a relatively small value of the initial state variable (see Table 1), only because we are interested to the crack propagation and in order to reduce the computational times of the nucleation stage. We have verified, however, that our results do not depend on this assumption and that similar traction and slip velocity behaviors have been obtained using larger initial values of the state variable. Figure 10 also shows that for small value of v_{init} we have high values of the yield stress and larger equivalent SW distances. The correspondence between the modeled and the theoretical (resulting from equation 10) values of d_0^{eq} is shown in the panels of Figures 6 and 10a. In Figure 10b we plot the traction as a function of slip rate (in a log scale) to emphasize the contribution of the direct effect of friction and the different steady state friction values (for $v = v_0$) in each configuration.

[28] In conclusion, we note that the slip velocity and the state variable values (v_u and Φ_u) appearing in equation (14) depend on the adopted a, b, and L values as well as on the initial slip velocity. Therefore the dependence of the yield stress on the constitutive parameters is quite complex. The same is true for the slip velocity value v_0. While we are able to derive an analytical expression for the equivalent SW distance and for the kinetic friction expressing the dependence on the constitutive parameters found in numerical simulations, the same cannot be easily done for the yield stress.

8. Discussion

[29] The simulations discussed above have been performed using a fault parameterization at the laboratory scale dimension, adopting values of constitutive parameters derived from laboratory experiments. A major problem that we have therefore to face is the scaling of our results from laboratory to actual fault dimensions. We have used in our calculations values of the L parameter ranging between 1 and 10 μm and, according to the derived scaling law (equation (10)), we found values of the equivalent slip-weakening distance comprised between 0.02 and 0.2 mm, or in general $d_0^{\text{eq}} < 1$ mm when we use a different initial state for the state variable (as in equation (9)). These values are much smaller than those recently proposed for actual faults and constrained by modeling ground motion waveforms recorded during large earthquakes [see *Guatteri et al.*, 2001, and reference therein]. In fact, recent investigations have proposed d_0 values larger than 0.2 m [*Ide and Takeo*, 1997; *Olsen et al.*, 1997]. A first solution to this problem consists in assuming the scaling from laboratory-derived values to those appropriate for earthquake fault dimension. We thus consider L to be of the order of 1 cm for actual faults [*Scholz*, 1988]; this implies to scale the L values obtained in laboratory, for instance during experiments with gauge materials [see *Mair and Marone*, 1999] to real faults. According to the proposed scaling law, this would yield critical slip-weakening values of $d_0^{\text{eq}} \sim 0.2$ m ($d_0^{\text{eq}} < 0.5$ m) in agreement with observations. However, it must be pointed out that there exist several concerns about the reliability of such large values of the critical slip-weakening distance: *Guatteri and Spudich* [2000] discussed this topic and concluded that estimates of SW distance inferred from kinematic inversions of seismograms are biased because of the trade-off between strength excess and slip-weakening distance and because of the effects of smoothing constraints used in inversion algorithms. *Marone and Kilgore* [1993] suggested that the critical slip distance is controlled by the
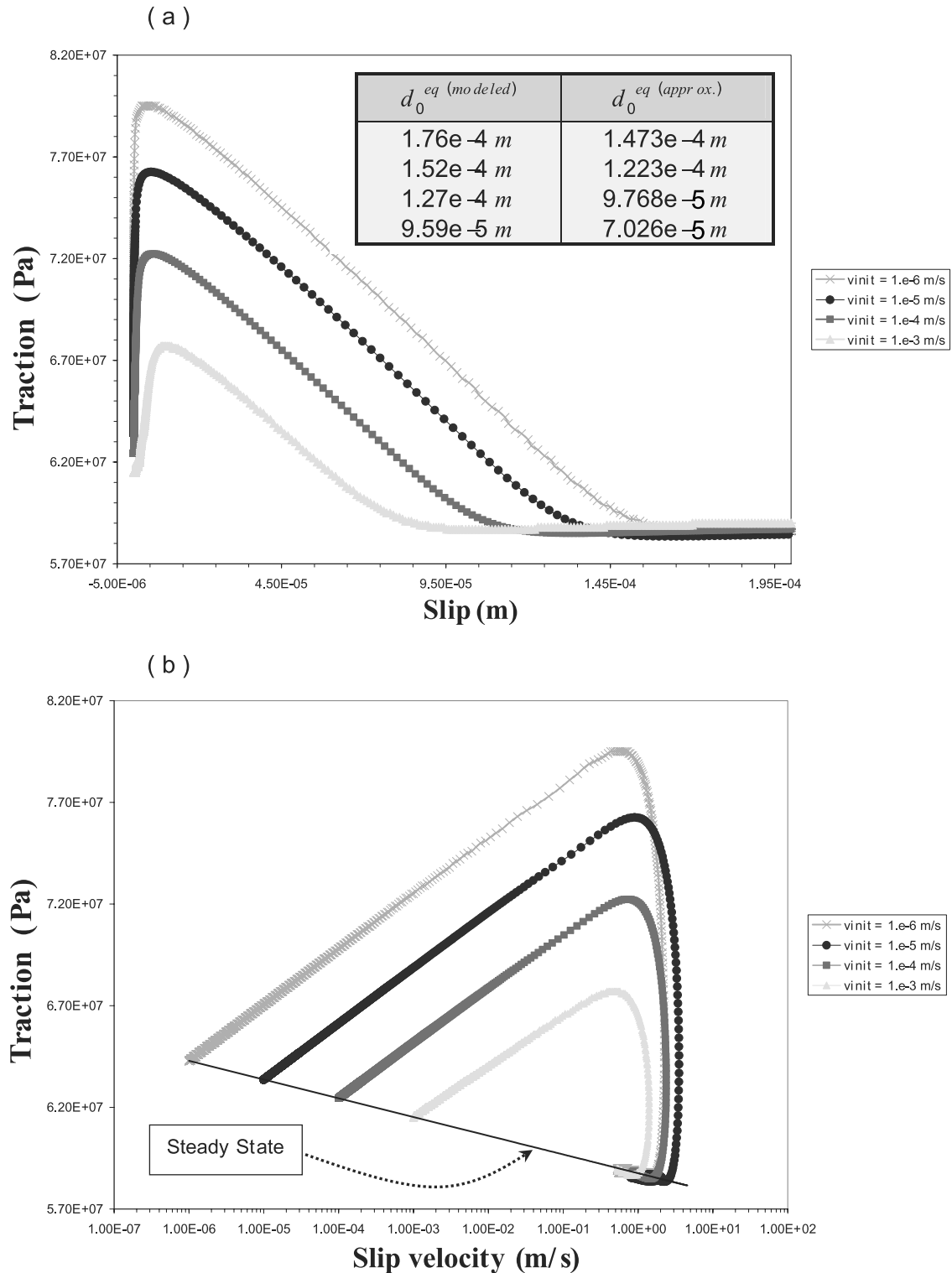
(a)

(b)

Figure 10. Dependence of total dynamic traction on the adopted initial slip velocity v_{init}. (a) The usual SW curves computed using different values of the initial velocity keeping fixed all the other constitutive parameters and the fault discretization. (b) The dynamic traction as a function of the logarithm of slip velocity for different v_{init}. The straight line in this logarithmic plot indicates the steady friction. By changing the initial velocity we modify the initial value of the state variable ($\Phi_{init} = \Phi^{ss}(v_{init}) = L/v_{init}$). The box in Figure 10a lists the values of the equivalent characteristic SW distance (d_0^{eq}) resulting from the numerical modeling and those inferred from the approximated relation (equation (10)).
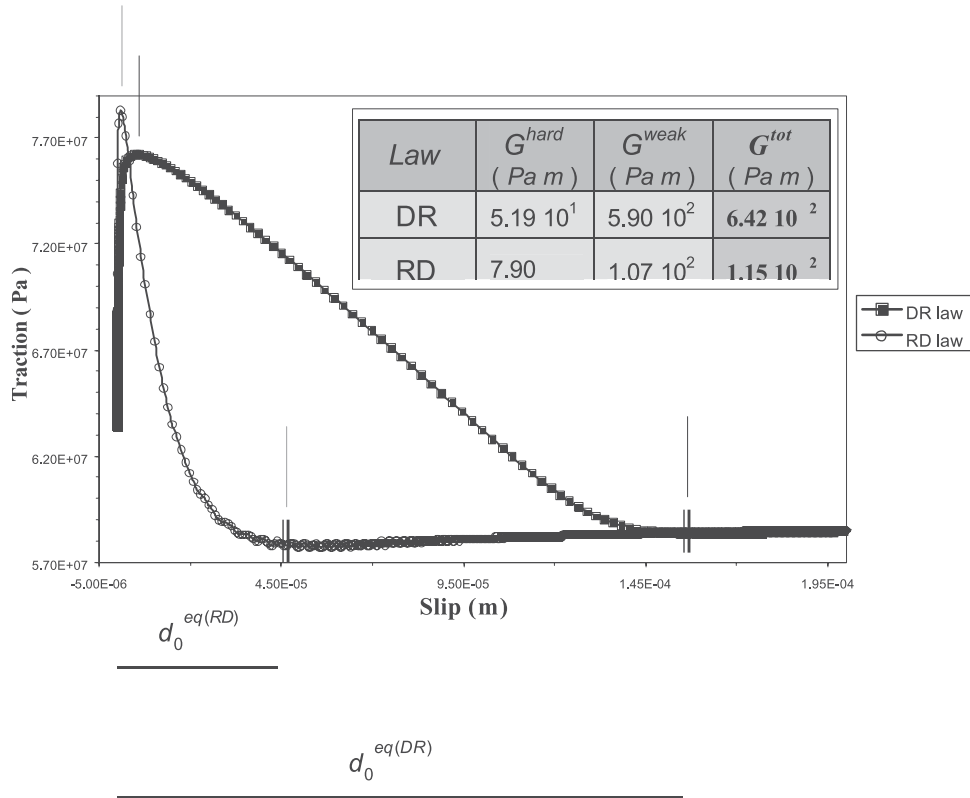
Figure 11. Comparison between the slip-weakening curve computed using a slowness (used in all previous simulations; DR equations (3)) and slip evolution law (RD; equations (4)) for the same constitutive parameters and initial conditions.

thickness of the fault zone of localized shear strain. Therefore the discrepancy between laboratory measurements and values obtained from modeling earthquakes might be attributed both to the differences in roughness between laboratory surfaces and natural faults [*Scholz*, 1988] as well as in the thickness of the localized shear strain zone [*Marone and Kilgore*, 1993].

[30] The numerical results presented in this study demonstrate that the state variable evolution controls the absorbed fracture energy and the traction drop within the cohesive zone. Our simulations suggest that the adopted evolution law characterizing the state variable and the rate- and state-constitutive parameters produce different traction evolutions and slip-weakening behaviors. In order to understand how the analytical expression adopted for the evolution law in the RS formulation affects the traction evolution within the cohesive zone, we have performed a set of simulations using slowness and slip evolution laws (equations (3) and (4)). In particular, we use the rate- and state-dependent slip law [see *Ruina*, 1983; *Beeler et al.*, 1994] in the formulation proposed by *Roy and Marone* [1996] as defined in equation (4). We show in Figure 11 the comparison between the SW curve resulting from a slip and a slowness evolution law, keeping fixed all the constitutive and initial parameters. In these simulations the evolution law is different, while the governing equation for fault friction is nearly the same. Figure 11 shows that the SW behavior and the equivalent slip-weakening distance depend on the analytical expression adopted for the evolution law. The characteristic SW distance is strongly reduced (roughly

by a factor 3) when a slip evolution law is used. The weakening rate for a slip evolution law is not constant, which results in a nonlinear decay, the opposite of what observed with a slowness evolution law. An evident traction roll-off characterizes the traction evolution for slip values near to the equivalent slip-weakening distance. The kinetic friction level is exactly the same, confirming that the final steady state value is unchanged, but the yield stress is different. This implies that the fracture energy resulting from the simulations performed with these two distinct evolution laws is different: a slip law involves fracture energy five times smaller than that resulting from a slowness law. This result further confirms that the evolution law and the state variable control the traction drop and the finite fracture energy absorption at the crack tip.

[31] Several papers were recently aimed to discuss the implications of the adopted analytical formulation of rate- and state-dependent friction laws [see *Roy and Marone*, 1996; *Belardinelli et al.*, 2003; *He et al.*, 2003, and references therein]. Most of them focused on the different expressions adopted for the evolution law. In the present study we deal with the traction evolution within the cohesive zone and in particular with the slip-weakening behavior intrinsic in the RS formulation. The results shown in Figure 11 further emphasize the problem of the most appropriate analytical representation of friction. It is important to remark that these constitutive laws attempt to provide a macroscopic representation of frictional process. In the literature, the evolution law and the state variable have been interpreted in different ways. The most widely adopted

interpretation consists in assuming that the state variable represents the properties and the roughness of the contact surface, but alternative interpretation have related the evolution law and the state variable to the porosity of fault zones [see *Segall and Rice*, 1995; *Sleep*, 1997]. In the present study we have shown that, in the framework of rate- and state-constitutive laws, the state variable evolution controls the weakening mechanisms characterizing the breakdown process. Although we can explain the traction evolution within the cohesive zone in terms of the state variable evolution, we cannot provide a unique physical interpretation of the shear stress degradation during the breakdown process. Moreover, other physical processes can contribute to the weakening mechanisms, such as thermal-weakening [*Sleep*, 1997], fluid pressurization [*Andrews*, 2002] or mechanical lubrication [*Brodsky and Kanamori*, 2001]. They certainly play a dominant role to explain the raise of pore pressure and the consequent reduction of frictional resistance. Therefore our opinion is that different phenomena can contribute to the traction evolution and the weakening mechanisms associated with the rupture growth, which can affect either the friction coefficient or the effective normal stress. The increase of fluid pressure reduces the effective normal stress, thus affecting the friction law. These phenomena may coexist, since the friction coefficient depends on slip, slip rate-and-state variables (see equation (3)) and pore pressure affects the effective normal stress. The solution of this problem is well above the goal of the present study. We only aim to contribute to the debate concerning the constitutive properties in the achievable perspective to find a unified constitutive law to describe the earthquake dynamic rupture growth.

9. Conclusions

[32] In this paper we have numerically solved the fully dynamic problem for a 2-D, in-plane, spontaneous fault, obeying rate- and state-dependent friction laws. We have shown that, in the framework of a RS-dependent constitutive formulation, the traction drop for increasing slip (i.e., the slip-weakening behavior) occurring within the cohesive zone during the dynamic rupture propagation is controlled by the state variable evolution, which drives the fast slip acceleration. The characteristic length scale parameter of a dynamic rupture obeying a RS constitutive law (i.e., the parameter L) is different from the critical (named here "equivalent") slip-weakening distance d_0^{eq}. The characteristic SW parameters (the equivalent SW distance, the yield stress and the kinetic friction level) depend on the constitutive parameters of the RS formulation and the slip velocity values at particular stages of the breakdown process. The proposed scaling laws and analytical relations derived in this study allow to associate RS and SW constitutive parameters for modeling the spontaneous rupture propagation and arrest [see *Bizzarri et al.*, 2001; *Cocco and Bizzarri*, 2002] during a single earthquake rupture.

[33] We have demonstrated that the adopted evolution law affects the slip-weakening behavior. We have compared the SW curves resulting from slowness and slip evolution laws and we point out that the critical SW distance in these two cases is different. This result corroborates that the

state variable controls the traction behavior and the slip acceleration during the breakdown process. The main implications resulting from these considerations concern the absorbed fracture energy and the duration of the weakening process. A slip evolution law implies an extremely fast evolution of the state variable that produces large slip accelerations and perhaps unrealistic large peak slip velocities. We emphasize that a rate- and state-dependent formulation allows a quantitative description of the dynamic rupture nucleation, propagation and arrest [see also *Bizzarri et al.*, 2001]. Moreover, a slowness evolution law yields a very simple SW behavior, surprisingly similar to the classical constitutive law proposed by *Ida* [1972], and realistic behavior within the cohesive zone.

[34] The results presented in this study suggest that the temporal evolution of traction and slip velocity resulting from the adoption of a RS constitutive law is different from that resulting from a classical SW law. Both these constitutive representations of friction predict that the peak of dynamic traction occurs before the peak in slip velocity [see also *Olsen et al.*, 2001; *Mikumo et al.*, 2003]. However, the simulations performed in this study assuming a RS formulation clearly show that the peak slip velocity does not occur at the minimum traction (i.e., at the kinetic stress level). In other words, the value of slip velocity when the fault slip is equal to the slip-weakening distance is smaller than its peak value. This result restricts the possibility to evaluate the critical slip distance from near-field ground motion records, as recently proposed in the literature.

Appendix A: Convergence and Stability Conditions

[35] In this appendix we briefly summarize the convergence and stability conditions that have to be satisfied in order to correctly resolve the dynamic traction evolution and the slip velocity behavior within the cohesive zone during the propagation of a dynamic rupture obeying rate- and state-dependent friction laws. The first condition that has to be satisfied is a requirement introduced by *Rice* [1993] to demonstrate that artificial numerical complexity can appear if the medium is not correctly discretized as a continuum; it depends on the fault geometry and on the boundary conditions. In full of generality it can be expressed as $k_{diag} \gg k_{cr}$, where k_{diag} is the diagonal term of stiffness matrix and k_{cr} is the critical stiffness. The requirement $k_{diag} \gg k_{cr}$ corresponds to impose that locally each single element of the discretized fault is conditionally stable (*Scholz*, 1990). This avoids that a single point may fail independently of the neighbors (artificial complexity and numerical noise) and guarantees that the discrete medium can be considered as a continuum. The local stiffness is expressed as $k_{diag} = 1/C$, where C is the local compliance [*Andrews*, 1985]. C represents the proportionality constant between instantaneous traction and dynamic slip and in our 2-D FD fault model is

$$C = 3^{1/2} v_S \rho / (8 w_{CFL} \Delta t)$$

where w_{CFL} is the Courant-Friedrichs-Levy (CFL) ratio that relates Δx to Δt ($w_{CFL} = v_S \Delta t / \Delta x$ [see *Fukuyiama and Madariaga*, 1998; *Bizzarri et al.*, 2001]). The critical

stiffness can be expressed as $(b - a) \sigma_n^{\mathrm{eff}}/L$ [*Ranjith and Rice*, 1999], where the constitutive parameters a, b, σ_n^{eff} and L have been assigned. When $k_{\mathrm{diag}} = k_{\mathrm{cr}}$, we have the critical grid size:

$$\Delta t^* = \frac{v_S \rho L}{(b-a)\sigma_n^{\mathrm{eff}}} \frac{8}{\sqrt{3}} w_{\mathrm{CFL}}, \qquad (A1)$$

or, alternatively,

$$\Delta x^* = \frac{v_S^2 \rho L}{(b-a)\sigma_n^{\mathrm{eff}}} \frac{8}{\sqrt{3}}$$

The Rice condition can be therefore expressed as

$$\Delta t \ll \Delta t^*, \qquad (A2)$$

or, alternatively, as

$$\Delta x \ll \Delta x^*$$

For our purposes we have to verify also that the numerical integration is able to correctly resolve time scales typical of the dynamic evolution of the state variable. Following *Ohnaka and Yamashita* [1989] and *Cocco and Bizzarri* [2002], we define here the equivalent breakdown zone duration (or time) as T_b^{eq} and the equivalent cohesive zone size as X_b^{eq}. We remind here that during the breakdown time duration and over the cohesive zone distance the friction decreases from the maximum yield value to the kinetic level and, according to our interpretation, such a dynamic behavior is controlled by the state variable evolution. Therefore the requirement of resolution of this characteristic time duration and spatial scale consists to impose the following conditions:

$$\Delta t \ll \frac{d_0^{\mathrm{eq}}}{\langle v \rangle_{T_b^{\mathrm{eq}}}}, \qquad (A3a)$$

or, alternatively,

$$\Delta x \ll \frac{1}{w_{\mathrm{CFL}}} \frac{v_S}{\langle v \rangle_{T_b^{\mathrm{eq}}}} d_0^{\mathrm{eq}}$$

or, in a different way,

$$\Delta t \ll w_{\mathrm{CFL}} \frac{1}{v_S} \frac{v_{\mathrm{crack}}}{\langle v \rangle_{T_b^{\mathrm{eq}}}} d_0^{\mathrm{eq}}, \qquad (A3b)$$

or, alternatively,

$$\Delta x \ll \frac{v_{\mathrm{crack}}}{\langle v \rangle_{T_b^{\mathrm{eq}}}} d_0^{\mathrm{eq}}$$

where v_{crack} is the crack speed propagation and $\langle v \rangle_{T_b^{\mathrm{eq}}}$ is the average slip velocity calculated within the equivalent breakdown zone time (see *Bizzarri et al.* [2001] for further details).

[36] Finally, the spatial and time steps are coupled by the general condition [e.g., *Andrews*, 1985; *Fukuyama and Madariaga*, 1998]

$$\Delta x \geq v_p \Delta t, \qquad (A4)$$

which states that no coupling exists between first neighbors.

Appendix B: A Priori Estimation of Equivalent Slip-Weakening Parameters

[37] We have derived a set of approximated relations to express the equivalent slip-weakening distance (equations (9) and (10)), the equivalent kinetic friction level τ_f^{eq} (equation (13)) and the equivalent upper yield stress τ_u^{eq} (equation (14)) as a function of the RS constitutive parameters. We aim to use these equations to compare analytical predictions with estimates from numerical simulations. As pointed out in the text, these equations also depend on slip velocity and state variable values associated to particular stages of the breakdown process, which are a priori unknown (such as v_0, v_u and Φ_u; see Figure 2). One possible solution to overcome this limitation is to find useful equations relating these unknown slip velocity and state variable values to the final slip velocity value v_2 (see Figures 2a and 2b). These empirical relations depend on the adopted constitutive law and the parameters a, b, and L, as well as on v_{init}. We have verified that, for our set of constitutive parameters and initial conditions, the following empirical approximated relations hold:

$$\begin{aligned} v_0 &\cong 2v_2 \\ v_u &\cong 2v_2/3 \\ \Phi_u &\cong 2\Phi_{\mathrm{init}/3} \end{aligned} \qquad (B1)$$

where $\Phi_{\mathrm{init}} = L/v_{\mathrm{init}}$. The velocity v_2 is derived from the shear impedance relation [see, e.g., *Scholz*, 1990]:

$$\frac{v_2}{2v_S} = \frac{\Delta \tau_d}{\mu}, \qquad (B2)$$

where $\Delta \tau_d$ is the dynamic stress drop, defined as the difference existing between the initial and the final shear stress values [*Brune*, 1970]. This equation expresses the asymptotic level at which the slip velocity drops when the crack tip has propagated a sufficient distance beyond the target point, so that the influence of crack tip energy concentration is absent. We remark here that the friction at the end of phase IV (Figure 2c) is at the steady state and it is equal to $\tau^{ss}(v_2)$. Therefore we have

$$\Delta \tau_d = (b - a)\sigma_n^{\mathrm{eff}} \ln\left(\frac{v_2}{v_{\mathrm{init}}}\right). \qquad (B3)$$

The final velocity v_2 is therefore determined by solving the following transcendental equation:

$$\mu v_2 = 2v_S(b - a)\sigma_n^{\mathrm{eff}} \ln\left(\frac{v_2}{v_{\mathrm{init}}}\right) \qquad (B4)$$

from which we can simply obtain a rough estimate of the v_2 value, that depends on the difference $(b - a)$ and on the initial slip velocity. Once this slip velocity value is known, we can measure d_0^{eq}, τ_f^{eq}, and τ_u^{eq} through equations (10), (13), and (14) after expressing all the other unknown values in terms of v_2, by using the approximated relations proposed here (equations (B1)). This is a practical approach to have an a priori estimate of the equivalent slip-weakening parameters.

[38] We emphasize however that the approximated relations (B1) are valid only if the simulation starts form the steady state and if we adopt a slowness (ageing) evolution law.

References

Andrews, D. J., A numerical study of tectonic stress release by underground explosions, *Bull. Seismol. Soc. Am.*, 63, 1375–1391, 1973.

Andrews, D. J., Rupture propagation with finite stress in antiplane strain, *J. Geophys. Res.*, 81, 3575–3582, 1976a.

Andrews, D. J., Rupture velocity of plane strain shear cracks, *J. Geophys. Res.*, 81, 5679–5687, 1976b.

Andrews, D. J., Dynamic plane-strain shear rupture with a slip-weakening friction law calculated by a boundary integral method, *Bull. Seismol. Soc. Am.*, 75, 1–21, 1985.

Andrews, D. J., Test of two methods for faulting in finite-difference calculations, *Bull. Seismol. Soc. Am.*, 89, 931–937, 1999.

Andrews, D. J., A fault constitutive relation accounting for thermal pressurization of pore fluid, *J. Geophys. Res.*, 107(B12), 2363, doi:10.1029/2002JB001942, 2002.

Barenblatt, G. I., Concerning equilibrium crack forming during brittle fracture: The stability of isolated cracks: Relationship with energetic theories, *Appl. Math. Mech.*, 23, 1273–1282, 1959.

Beeler, N. M., and T. E. Tullis, Self-healing slip pulses in dynamic rupture models due to velocity-dependent strength, *Bull. Seismol. Soc. Am.*, 86, 1130–1148, 1996.

Beeler, N. M., T. E. Tullis, and J. D. Weeks, The roles of time and displacement in the evolution effect in rock friction, *Geophys. Res. Lett.*, 21, 1987–1990, 1994.

Belardinelli, M. E., A. Bizzarri, and M. Cocco, Earthquake triggering by static and dynamic stress changes, *J. Geophys. Res.*, 108(B3), 2135, doi:10.1029/2002JB001779, 2003.

Bizzarri, A., M. Cocco, D. J. Andrews, and E. Boschi, Solving the dynamic rupture problem with different numerical approaches and constitutive laws, *Geophys. J. Int.*, 144, 656–678, 2001.

Boatwright, J., and M. Cocco, Frictional constraints on crustal faulting, *J. Geophys. Res.*, 101, 13,895–13,909, 1996.

Brodsky, E. E., and H. Kanamori, Elastohydrodynamic lubrication of faults, *J. Geophys. Res.*, 106, 16,357–16,374, 2001.

Brune, J. N., Tectonic stress and the spectra of seismic shear waves from earthquakes, *J. Geophys. Res.*, 75, 4997–5009, 1970.

Cocco, M., and A. Bizzarri, On the slip-weakening behavior of rate- and state dependent constitutive laws, *Geophys. Res. Lett.*, 29(11), 1516, doi:10.1029/2001GL013999, 2002.

Das, S., and K. Aki, A numerical study of two-dimensional spontaneous rupture propagation, *Geophys. J. R. Astron. Soc.*, 50, 643–668, 1977a.

Das, S., and K. Aki, Fault plane with barriers: a versatile earthquake model, *J. Geophys. Res.*, 82, 5658–5670, 1977b.

Dieterich, J. H., Modeling of rock friction: 1. Experimental results and constitutive equations, *J. Geophys. Res.*, 84, 2161–2168, 1979.

Dieterich, J. H., A model for the nucleation of earthquake slip, in *Earthquake Source Mechanics*, *Geophys. Monogr. Ser.*, vol. 37, edited by S. Das, J. Boatwright, and C. H. Scholz, pp. 37–47, AGU, Washington, D.C., 1986.

Dieterich, J. H., Earthquake nucleation on faults with rate- and state-dependent strength, *Tectonophysics*, 211, 115–134, 1992.

Dieterich, J. H., and B. D. Kilgore, Direct observations of frictional contacts: New insights for state-dependent properties, *Pure Appl. Geophys.*, 143(1–3), 283–302, 1994.

Fukuyama, E., and R. Madariaga, Rupture dynamics of a planar fault in a 3-D elastic medium: rate- and slip-weakening friction, *Bull. Seismol. Soc. Am.*, 88, 1–17, 1998.

Gu, Y., and T.-F. Wong, Effects of loading velocity, stiffness, and inertia on the dynamics of a single degree of freedom spring-slider system, *J. Geophys. Res.*, 96, 21,677–21,691, 1991.

Guatteri, M., and P. Spudich, What can strong-motion data tell us about slip-weakening fault-friction laws?, *Bull. Seismol. Soc. Am.*, 90, 98–116, 2000.

Guatteri, M., P. Spudich, and G. C. Beroza, Inferring rate and state friction parameters from rupture model of the 1995 Hyogo-ken Nambu (Kobe) Japan earthquake, *J. Geophys. Res.*, 106, 26,511–26,522, 2001.

He, C., T.-f. Wong, and N. M. Beeler, Scaling of stress drop with recurrence interval and loading velocity for laboratory-derived fault strength relations, *J. Geophys. Res.*, 108(B1), 2037, doi:10.1029/2002JB001890, 2003.

Ida, Y., Cohesive force across the tip of a longitudinal-shear crack and Griffith's specific surface energy, *J. Geophys. Res.*, 77, 3796–3805, 1972.

Ide, S., and M. Takeo, Determination of constitutive relations of fault slip based on seismic wave analysis, *J. Geophys. Res.*, 102, 27,379–27,391, 1997.

Lapusta, N., J. R. Rice, Y. Ben-Zion, and G. Zheng, Elastodynamic analysis for slow tectonic loading with spontaneous rupture episodes on faults with rate- and state- dependent friction, *J. Geophys. Res.*, 105, 23,765–23,789, 2000.

Mair, K., and C. J. Marone, Friction of simulated fault gauge for a wide range of velocities and normal stresses, *J. Geophys. Res.*, 104, 28,889–28,914, 1999.

Marone, C. J., and B. Kilgore, Scaling of the critical slip distance for seismic faulting with shear strain in fault zones, *Nature*, 362, 618–621, 1993.

Mikumo, T., E. Fukuyama, K. B. Olsen, and Y. Yagi, Stress-breakdown time and critical weakening slip inferred from slip-velocity on earthquake faults, *Bull. Seismol. Soc. Am.*, 93, 264–293, 2003.

Ohnaka, M., Nonuniformity of the constitutive law parameters for shear rupture and quasistatic nucleation to dynamic rupture: a physical model of earthquake generation processes, *Proc. Natl. Acad. Sci. U.S.A.*, 93, 3795–3802, 1996.

Ohnaka, M., and L. F. Shen, Scaling of the shear rupture process from nucleation to dynamic propagation: Implications of geometric irregularity of the rupturing surfaces, *J. Geophys. Res.*, 104, 817–844, 1999.

Ohnaka, M., and T. Yamashita, A cohesive zone model for dynamic shear faulting based on experimentally inferred constitutive relation and strong motion source parameters, *J. Geophys. Res.*, 94, 4089–4104, 1989.

Ohnaka, M., Y. Kuwahara, and K. Yamamoto, Constitutive relations between dynamic physical parameters near a tip of the propagating slip zone during stick-slip shear failure, *Tectonophysics*, 144, 109–125, 1987.

Okubo, P. G., Dynamic rupture modeling with laboratory-derived constitutive relations, *J. Geophys. Res.*, 94, 12,321–12,335, 1989.

Okubo, P. G., and J. H. Dieterich, Effects of physical fault properties on frictional instabilities produced on simulated faults, *J. Geophys. Res.*, 89, 5817–5827, 1984.

Olsen, K. B., R. Madariaga, and R. J. Archuleta, Three-dimensional dynamic simulation of the 1992 Landers earthquake, *Science*, 278, 834–838, 1997.

Olsen, K. B., E. Fukuyama, and T. Mikumo, Direct measurement of the slip-weakening distance from near-fault strong motion data, *Eos Trans. AGU*, 82(47), Fall Meet. Suppl., Abstract S21E-08, 2001.

Palmer, A. C., and J. R. Rice, The growth of slip surfaces in the progressive failure of over consolidated clay, *Proc. R. Soc. London, Ser. A*, 332, 527–548, 1973.

Perrin, G., J. R. Rice, and G. Zheng, Self-healing slip pulse on a frictional surface, *J. Mech. Phys. Solids*, 43, 1461–1495, 1995.

Ranjith, K., and J. R. Rice, Stability of quasi-static slip in a single degree of freedom elastic system with rate and state dependent friction, *J. Mech. Phys. Solids*, 47, 1207–1218, 1999.

Rice, J. R., Spatiotemporal complexity of slip on a fault, *J. Geophys. Res.*, 98, 9885–9907, 1993.

Roy, M., and C. Marone, Earthquake nucleation on model faults with rate- and state-dependent friction: effects of inertia, *J. Geophys. Res.*, 101, 13,919–13,932, 1996.

Ruina, A. L., Friction laws and instabilities: A quasistatic analysis of some dry frictional behavior, Ph. D., thesis, Brown Univ., Providence, R.I., 1980.

Ruina, A. L., Slip instability and state variable friction laws, *J. Geophys. Res.*, *88*, 10,359–10,370, 1983.

Scholz, C. H., Earthquakes and friction laws, *Nature*, *336*, 37–42, 1988.

Scholz, C. H., *The Mechanics of Earthquake and Faulting*, Cambridge Univ. Press, New York, 1990.

Segall, P., and J. R. Rice, Dilatancy, compaction, and slip instability of a fluid-infiltrated fault, *J. Geophys. Res.*, *100*, 22,155–22,171, 1995.

Sleep, N. H., Application of a unified rate and state friction theory to the mechanics of fault zones with strain localization, *J. Geophys. Res.*, *102*, 2875–2895, 1997.

—————————————

A. Bizzarri, Istituto Nazionale di Geofisica e Vulcanologia, Sede di Bologna, Sezione di Sismologia e Tettonofisica, Via Donato Creti, 12, I-40128 Bologna, Italy. (bizzarri@bo.ingv.it)

M. Cocco, Istituto Nazionale di Geofisica e Vulcanologia, Sezione di Sismologia e Tettonofisica, Via Di Vigna Murata, 605, I-00143 Rome, Italy. (cocco@ingv.it)